AD-A079 423 OHIO STATE UNIV COLUMBUS ELECTROSCIENCE LAB F/G 17/9
BASIC RESEARCH IN THREE-DIMENSIONAL IMAGING FROM TRANSIENT RADA--ETC(U)
JUN 79 J D YOUNG DASG60-77-C-0133
UNCLASSIFIED ESL-784785-5 NL

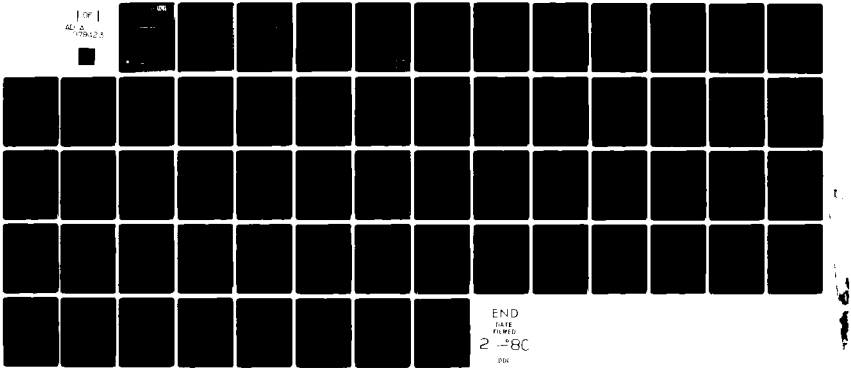

END
DATE FILMED
2-80
DDC

LEVEL II

OSU

The Ohio State University

BASIC RESEARCH IN THREE-DIMENSIONAL IMAGING FROM TRANSIENT RADAR SCATTERING SIGNATURES

Jonathan D. Young

The Ohio State University

ElectroScience Laboratory

Department of Electrical Engineering
Columbus, Ohio 43212

Final Report 784785-5

Contract DASG60-77-C-0133

June 1979

Ballistic Missile Defense Systems Command
Contracts Office BMDSC-CRS
P.O. Box 1500, Code W31RPD
Huntsville, Alabama 35807

79 11 09

NOTICES

When Government drawings, specifications, or other data are used for any purpose other than in connection with a definitely related Government procurement operation, the United States Government thereby incurs no responsibility nor any obligation whatsoever, and the fact that the Government may have formulated, furnished, or in any way supplied the said drawings, specifications, or other data, is not to be regarded by implication or otherwise as in any manner licensing the holder or any other person or corporation, or conveying any rights or permission to manufacture, use, or sell any patented invention that may in any way be related thereto.

SECURITY CLASSIFICATION OF THIS PAGE *(When Data Entered)*

REPORT DOCUMENTATION PAGE

READ INSTRUCTIONS BEFORE COMPLETING FORM

1 REPORT NUMBER

2. GOVT ACCESSION NO.

3. RECIPIENT'S CATALOG NUMBER

4. TITLE *(and Subtitle)*

(6) BASIC RESEARCH IN THREE-DIMENSIONAL IMAGING FROM TRANSIENT RADAR SCATTERING SIGNATURES.

5. TYPE OF REPORT & PERIOD COVERED
Final Report
7/1/77-3/31/79

6. PERFORMING ORG. REPORT NUMBER
ESL-784785-5

7. AUTHOR(s)

(10) Jonathan D. Young

8. CONTRACT OR GRANT NUMBER(s)
(14) Contract DASG60-77-C-0133 (15)

9. PERFORMING ORGANIZATION NAME AND ADDRESS
The Ohio State University ElectroScience Laboratory, Department of Electrical Engineering
Columbus, Ohio 43212

10. PROGRAM ELEMENT, PROJECT, TASK AREA & WORK UNIT NUMBERS
6.33.04.A. (12) 61

11. CONTROLLING OFFICE NAME AND ADDRESS
Ballistic Missile Defense Systems Command
Contracts Office BMDSC-CRS, P.O. Box 1500,
Code W31RPD, Huntsville, Alabama 35807

(11)

12. REPORT DATE
Jun[redacted]79

13. NUMBER OF PAGES
57

14. MONITORING AGENCY NAME & ADDRESS *(if different from Controlling Office)*

15. SECURITY CLASS. *(of this report)*
Unclassified

15a. DECLASSIFICATION/DOWNGRADING SCHEDULE

16. DISTRIBUTION STATEMENT *(of this Report)*

DISTRIBUTION STATEMENT A
Approved for public release;
Distribution Unlimited

17. DISTRIBUTION STATEMENT *(of the abstract entered in Block 20, if different from Report)*

(9) Final rept. 1 Jul 77-31 Mar 79

DDC RECEIVED JAN 15 1980 B

18. SUPPLEMENTARY NOTES

19. KEY WORDS *(Continue on reverse side if necessary and identify by block number)*

Radar signatures
Transient scattering
Inverse scattering
Radar target identification
Target imaging

20. ABSTRACT *(Continue on reverse side if necessary and identify by block number)*

The transient radar scattering signatures of a set of cone-like objects were studied, and techniques for creation of images using these signatures were investigated. The signatures were obtained from model measurements on two coherent 10:1 bandwidth complex scattering cross-section measurement systems. Ramp response signatures were generated from the measured data, and their relationship to target geometrical

DD FORM 1 JAN 73 1473 EDITION OF 1 NOV 65 IS OBSOLETE

402 251

SECURITY CLASSIFICATION OF THIS PAGE *(When Data Entered)*

20.

characteristics were analyzed. Two techniques for imaging from the signatures gathered at near nose-on look angles were investigated: Limiting Surface Imaging and Physical Optics Inverse Diffraction. Useful images, with some loss of detail, were produced.

CONTENTS

I. INTRODUCTION

This report describes the results of an 18 month project (with a 3 month no-cost extension) concerned with research on target imaging from radar echo data from cone-like targets. The contents of an interim report (Reference 1), three technical reports (References 2, 3, 4), and a published paper (Reference 5) are summarized.

Background for this research effort were techniques for radar target imaging and target identification which had been developed at Ohio State University and elsewhere (References 6-20). In general, such imaging techniques can be classified in two categories: low frequency techniques (interrogating signal wavelengths greater than one half the target maximum dimension) where gross target outlines are obtained, and interpretation is straight-forward but data measurement is difficult; and high frequency techniques (interrogating signal wavelengths much less than the target maximum dimension) where great quantities of information can be produced but interpretation is difficult.

The specific goals of this research effort were:

1. Obtaining transient response data which contains both high frequency and low-frequency radar scattering information for some target(s) of practical and scientific interest.

2. Performing image generation from the transient signature information, using both high frequency and low frequency approaches.

3. Further study of geometrical information which can be extracted from low-frequency, high-frequency, and polarization characteristics of target transient radar signatures.

4. Comparison and reinterpretation of the two types of imaging when they are applied using signature information applicable to both approaches. Specific identification of similarities and differences in the techniques.

A set of targets was chosen early in the program and measurements of complex radar cross section were made. All of these topics are summarized in Chapter II.

From the measured data, transient responses were synthesized and limiting surface images were generated for each target. Several improvements in this low frequency imaging approach were made during the course of the effort. The advances in the technique and resulting images are discussed in Chapter III.

Chapter IV contains the summary of our research on high frequency imaging and the comparison of the two imaging approaches. Physical optics inverse diffraction was the area chosen for concentrated study. Two- and three-dimensional image information for pertinent targets are included. Also, some target identification aspects of this effort are discussed.

Another research effort at this Laboratory has concentrated on the generation of electromagnetic transient signatures by laser stimulation of the metallic target. The relation of this work to radar target imaging is discussed in Chapter V.

Finally a summary of the effort and its most important results, and discussion of areas for future research are contained in Chapter VI.

II. TRANSIENT RESPONSE MEASUREMENTS

Measured scattering signature data formed the basis for much of the research effort on this contract. At the beginning, a set of cone target shapes was selected for measurement. These are shown in Figure 1. What was needed was measured impulse, step, and ramp response waveforms for these targets. Technical report 784785-3 discussed in detail the measured data, and the systems used to obtain it. A brief summary is included here.

Transient response data can be obtained by direct time-domain measurement, or by complex cross section measurements over a broad bandwidth (at least 10:1) in the frequency-domain and calculation of the inverse Fourier transform. The latter technique was used in this effort. Two frequency-domain systems, both covering the range of about 1 to 12 GHz, were used in the measurements. A very sensitive 10-frequency (1.08, 2.18, ... 10.8 GHz) system was used to measure the response of a set of models 5 cm long. Then a swept-frequency system covering 1 to 8 GHz was used to measure a set of models 40 cm long. Using appropriate calibration factors, a composite signature data set with a 58:1 frequency bandwidth was produced.

A. Ten-frequency Radar System

A block diagram of the experimental ten-harmonic radar backscatter system (References 5 and 6) is shown in Figure 2. In this system a single L-band microwave source is used to harmonically generate a set of frequencies. The network analyzer receiver local oscillator is used to modulate the higher harmonics (balanced modulators), and also to modulate (lower sideband) the L-band signal going into the reference port of the network analyzer receiver head. The result is that the receiver head of the network analyzer downconverts each of the harmonically related backscattered signals to the same IF frequency. The output of

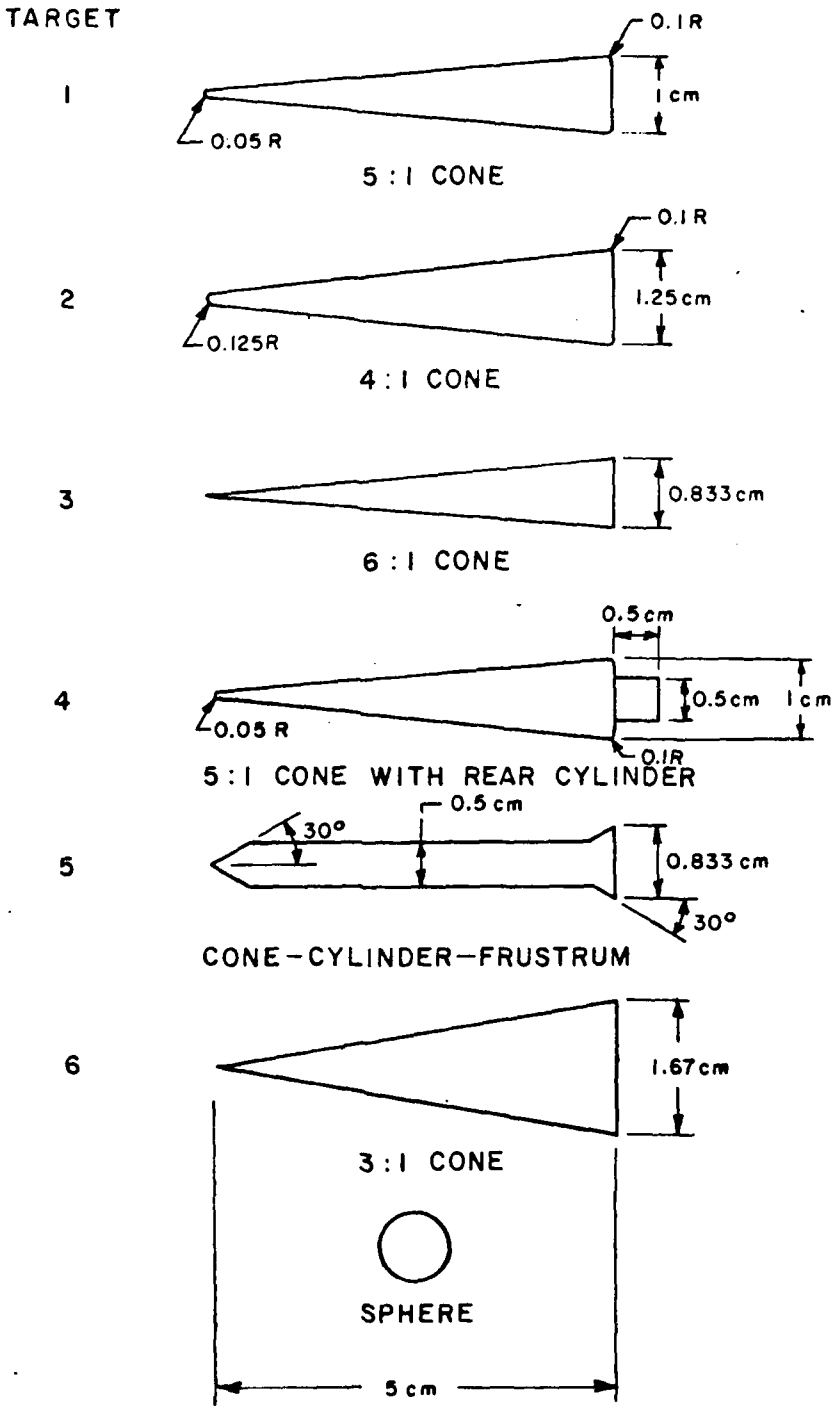

Figure 1. Outlines of targets used in this study.

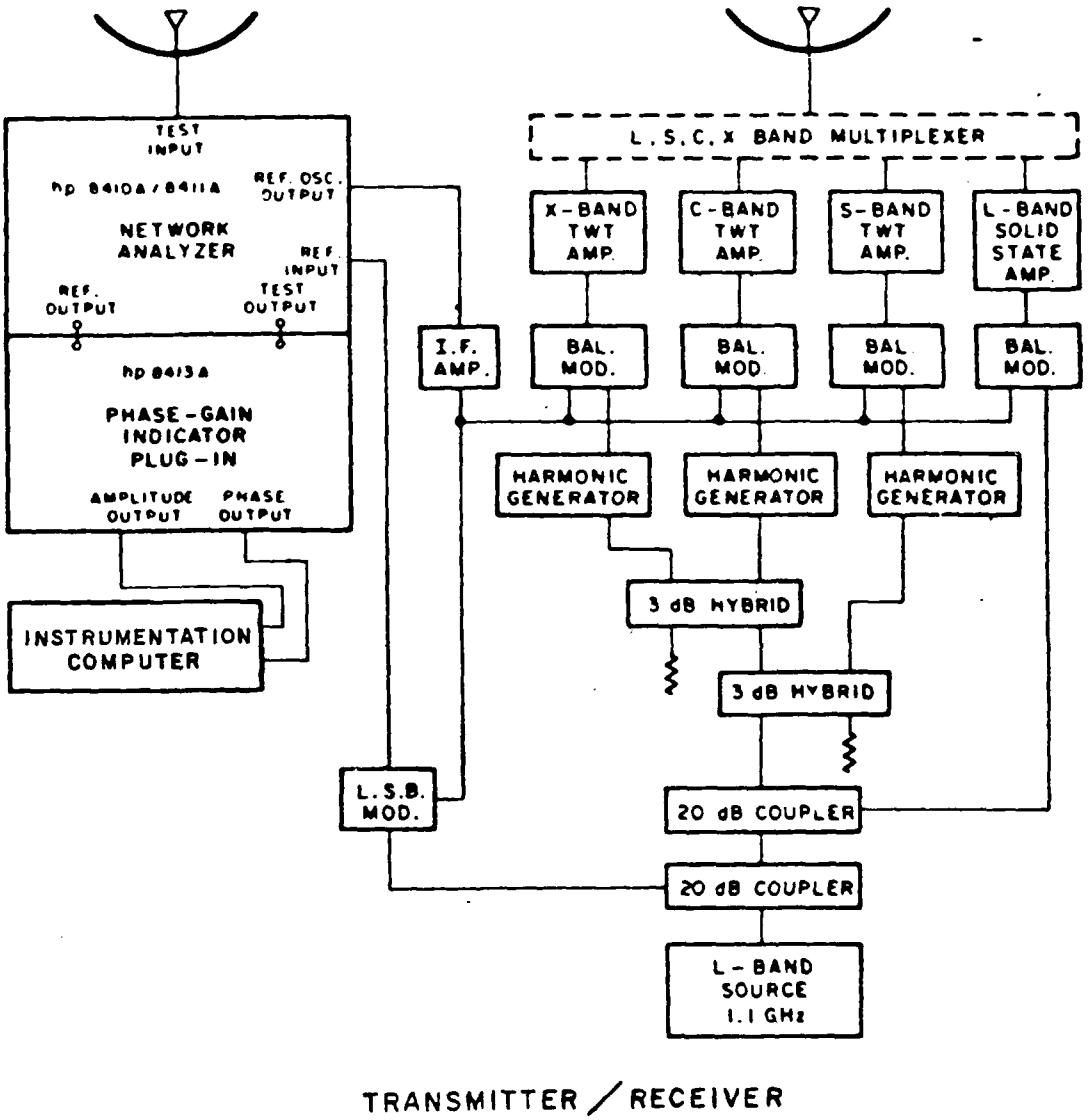

Figure 2. Block diagram of the ten-harmonic radar system.

the network analyzer is in fact, the vector sum of the set of signals being received. (In actual practice, the transmitter does not transmit all 10 harmonics simultaneously. Limitations in the transmitter output multiplexer require that the signals be transmitted in bands of 4 or 5 frequencies at a time.)

The processing of the data from this point reduces the contribution of the background and antenna coupling in the received signal and recovers the individual amplitude and phase of the individual harmonics. The operational procedure is to move the target slowly toward the radar antennas and to take amplitude and phase data samples under computer control. Arrays of amplitude and phase versus position data for the targets of interest as well as the empty support pedestal and a calibration and test sphere are stored in the computer. The raw data are Fourier transformed to yield the amplitude and phase of the individual harmonics. Any antenna coupling or scattering from stationary objects is rejected at this point as a DC term. The target measurements then have the empty pedestal (background) data subtracted and the final result is calibrated by using the calibration sphere data. In the end, we have the amplitude of the targets expressed as absolute radar cross section (in cm.) and the phase of the backscattered return relative to the center of the calibration sphere. The test sphere data serves as an estimate of the overall accuracy of the system.

In the initial stages of this project, a number of preliminary system checks and calibration tests were performed. It was necessary to confirm overall system linearity so that the Fourier techniques would not generate spurious results. It was also necessary to confirm the accuracy of the target positioning system so that the subtractions of the empty pedestal (background) data would be valid. The sensitivity and signal to noise behavior of the network analyzer also needed to be examined. Any degradation of the data at the low end of the dynamic range of the target and background measurements would clearly

cause severe errors in the results. The ten-harmonic range was finally considered to be functional, and a study of the overall system accuracy was undertaken, using the data on the test check sphere target. Some of the results are shown in Figure 3. In this figure, the amplitude and phase of the individual cross-sections for each harmonically related frequency are plotted using a polar format. As can be seen, the system produces data with accuracies on the order of 10%. (In this case, accuracy is defined as the magnitude of the error phasor divided by the magnitude of the known theoretical phasor.) As will be shown in the time domain section, this accuracy is sufficient for time domain analysis and imaging of the targets.

B. The Swept-Frequency Radar System

A block diagram of the swept frequency radar system is shown in Figure 4. This system is intended for larger target models than the ten frequency system, with data being obtained in finer increments in frequency. In such a system, the target would be stationary, and the signal to noise improvement introduced by the moving target data processing system would not be available. On the other hand, the targets would have radar cross sections approximately 64 times larger due to their 8 times larger dimensions. The basic concept of the swept frequency system and the steps in the measurement of the data are shown below.

(1) Measure and store in computer files amplitude and phase readings as the frequency is stepped over a band of frequency. Readings are taken on the targets, on reference and check spheres, and on the background.

(2) Subtract (phasor subtraction) the background data from the various target and sphere data to remove the errors due to various antenna coupling and unwanted scatter effects.

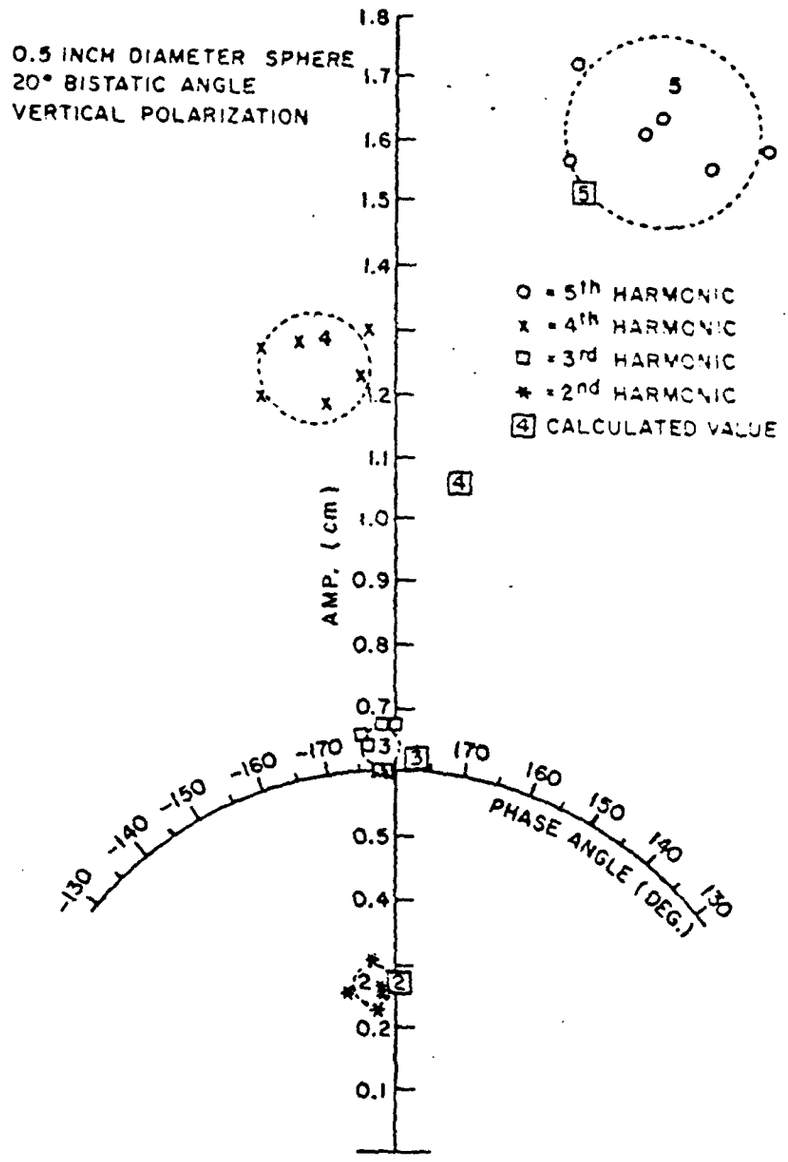

Figure 3. Polar diagram of measured scattering vs frequency for a test sphere.

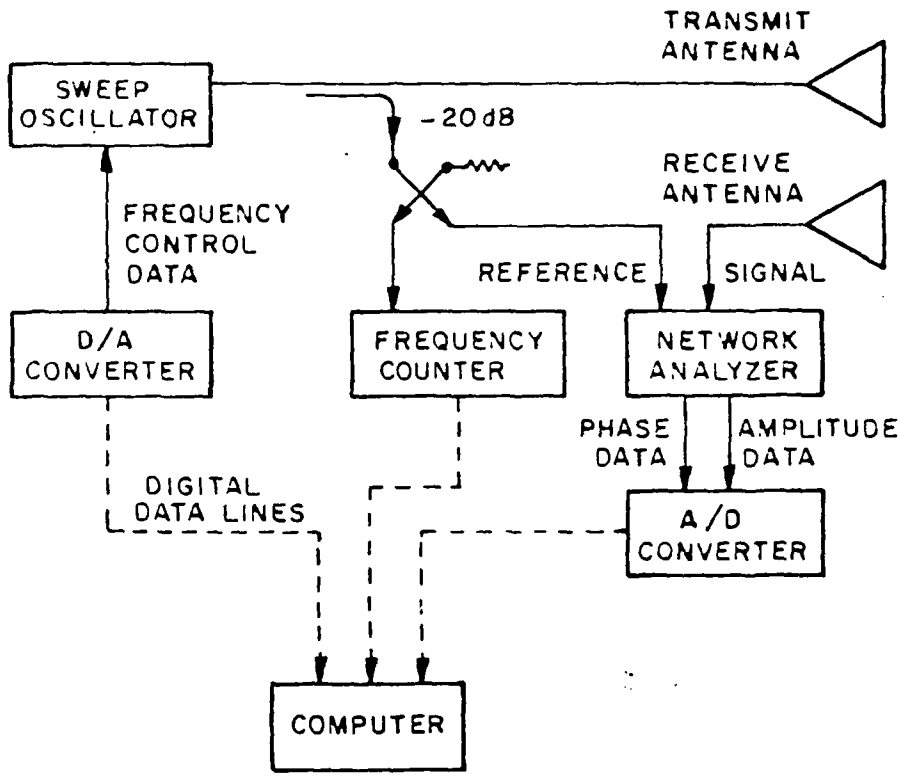

Figure 4. Block diagram of computer-controlled swept frequency radar system.

(3) Use computed values of the reference sphere to calibrate the system in terms of absolute radar backscatter cross section (amplitude and phase).

(4) Use data on the check sphere to confirm the overall integrity of the system and the data.

The major problem in the above set of concepts is due to constraints on the frequency repeatability of the swept frequency system. If the background is to be subtracted from the data on the various targets, then the frequency for each step in the frequency sweep must be repeatable to a high degree. The constraint is that the amplitude and phase of the background must be unchanged when the target is introduced. This can be assured if the set of data samples is taken at nearly identical frequencies for the background and for the set of targets. These qualitative requirements were studied early in this contract. As part of this study, measurements were made of the relationship between phase deviations due to frequency deviations and analog voltage variations due to frequency deviations. Typical results are;

Estimated phase accuracy requirement	= $\pm$ 5 deg.
Typical resultant frequency resolution	= $\pm$ 0.003 GHz
Resultant analog voltage accuracy	= $\pm$ 0.0088 volts/10 volts
Absolute voltage accuracy	= $\pm$ 1 part in 1100 (10 bits)

The analog voltage accuracy discussed in the above list is the voltage accuracy that would be needed if an analog voltage was used to control the frequency of the available microwave sweep frequency oscillator. This required voltage accuracy of (typically) 1 part in 1100 would require a design accuracy of perhaps 1 part in 2000 (11 bits). This stringent analog voltage stability and resolution requirement must be maintained even though the relationship between voltage and frequency is dependent on the sweep oscillator front panel dial settings. The analog system would require calibration each time the equipment was adjusted. It is these limitations which resulted in the decision to build a digital interface between the digital frequency counter and the computer. Experiments indicated that the drift in the internal oscillator in the frequency counter would not cause significant errors in the system. The output is inherently of high resolution (better than 5 decimal digits (1 part in 10,000) and requires no calibration at all. A computer flow

diagram of the software that was implemented to operate the digital frequency sweep system is shown in Figure 5. It has been shown that the total system satisfies the accuracy requirements presented above.

C. Typical Target Data

The measured complex cross-section vs harmonic for the nose-on look angle at targets 1 through 6 are shown in Figures 6 through 11 respectively. These data are normalized and calibrated to represent amplitude in square root of scattering area (in cm) and phase with respect to a phase center at the base of the cones, for frequencies of n (harmonic number) x 1.08 GHz impinging on the 5 cm long targets.

The physical optics assumption states that a ramp response waveform, obtained from these measured data by a Fast Fourier Transform with harmonic weighting of $1/n^2$ (n = harmonic number) should be proportional to cross-sectional area vs distance on the target, ahead of the shadow boundary (Reference 12). The nose-on ramp response waveforms, corresponding to the data in Figures 6 through 11, have been generated and analyzed. They are shown, after a base-line shift and removal of all portions except the time window of interest, in Figures 12 through 17. In each case, the actual cross sectional area vs distance of the target is also plotted for comparison. It is seen that the agreement is good for the front half of the target, with some lack of sharpness. Also, the ramp responses give a fair indication of the existence of the flat back surface, which is beyond the shadow boundary.

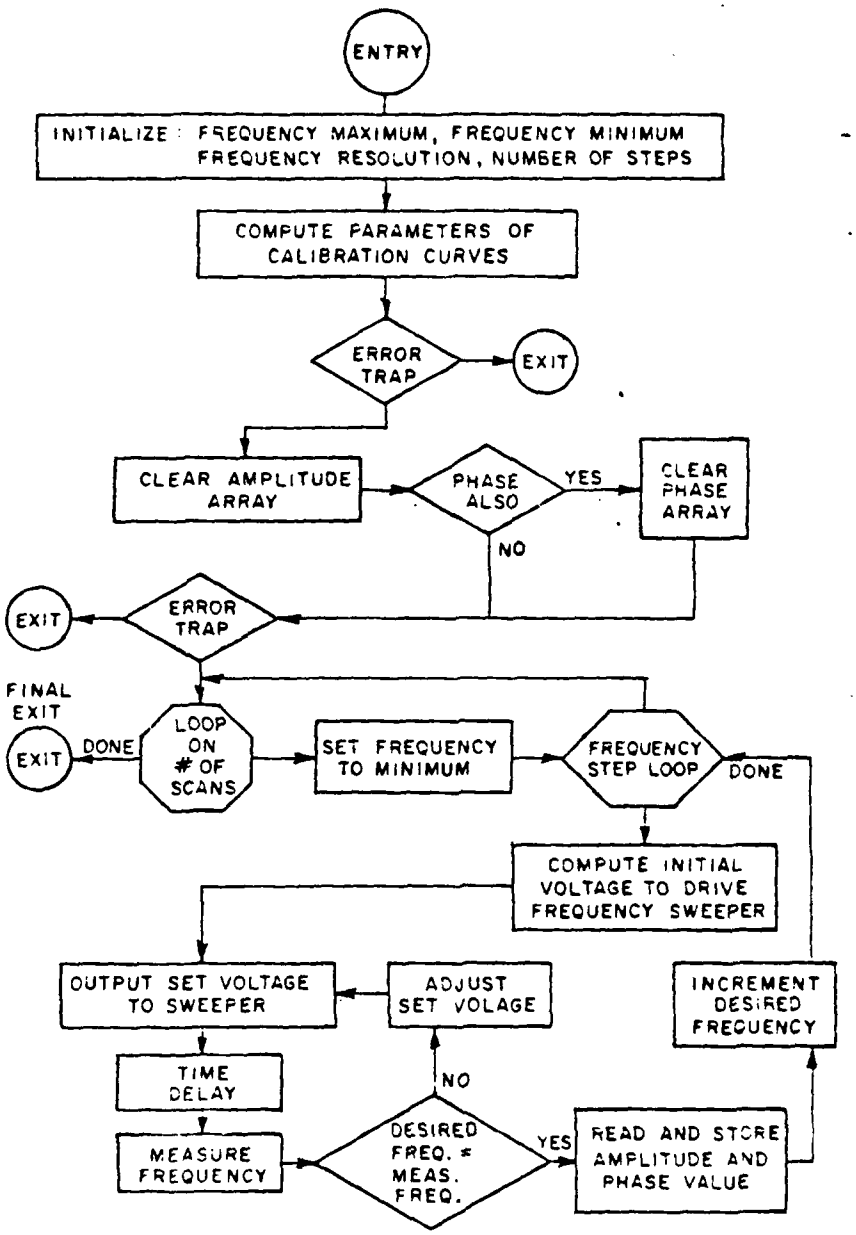

Figure 5. Flow diagram of computer-controlled swept frequency radar operation.

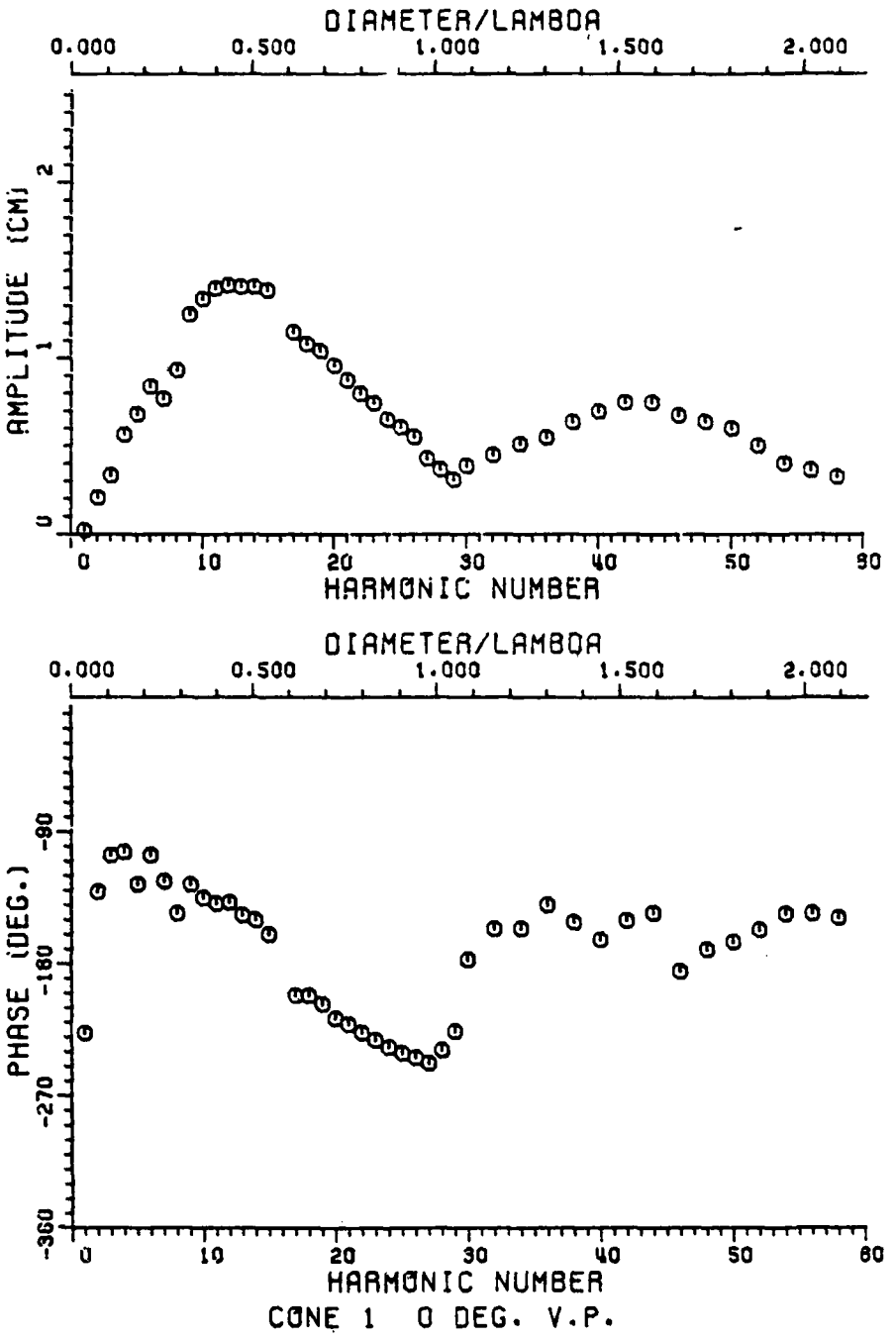

Figure 6. Complex scattering cross-section vs frequency nose-on incidence, Target #1.

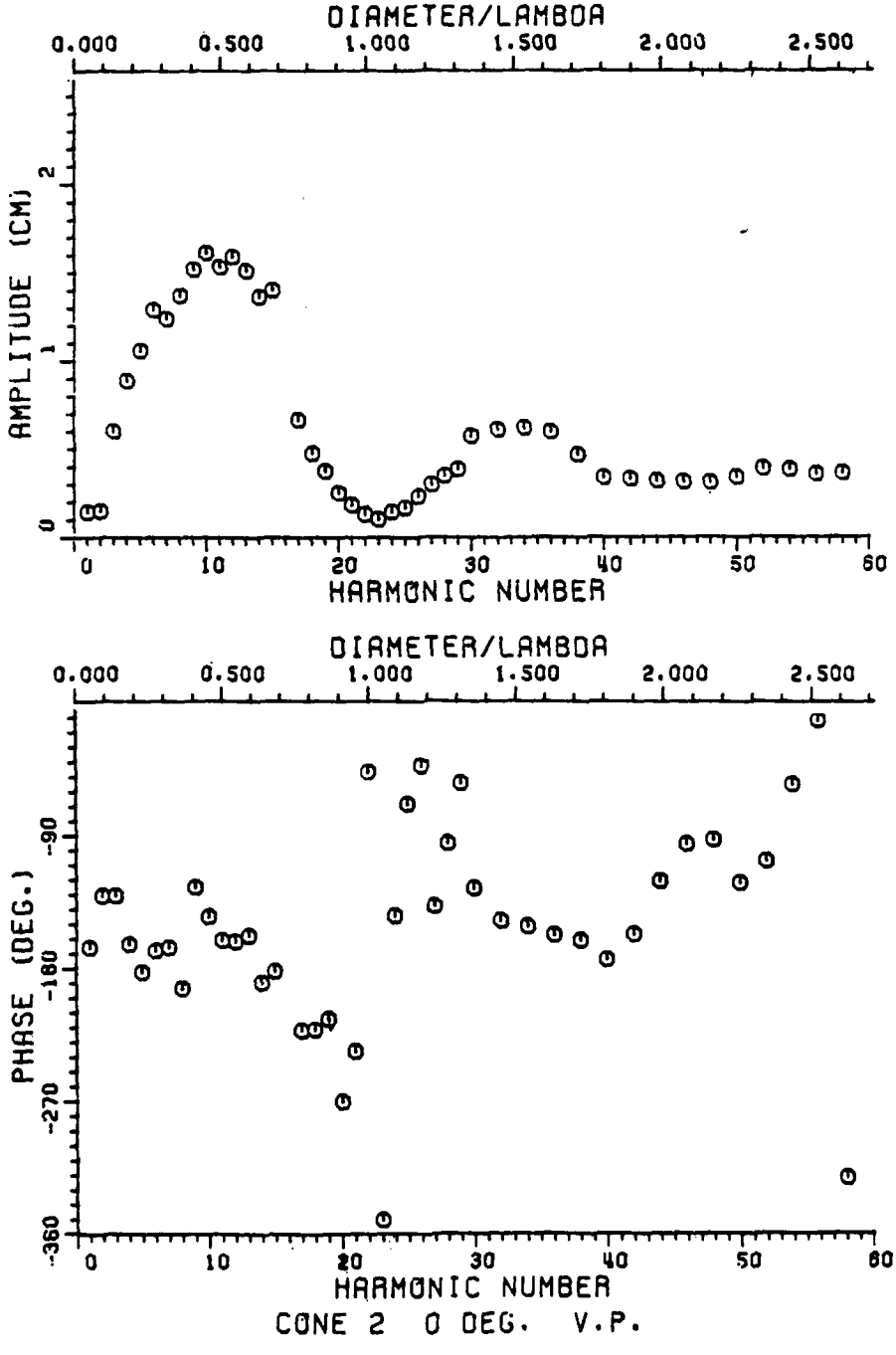

Figure 7. Complex scattering cross-section vs frequency nose-on incidence, Target #2.

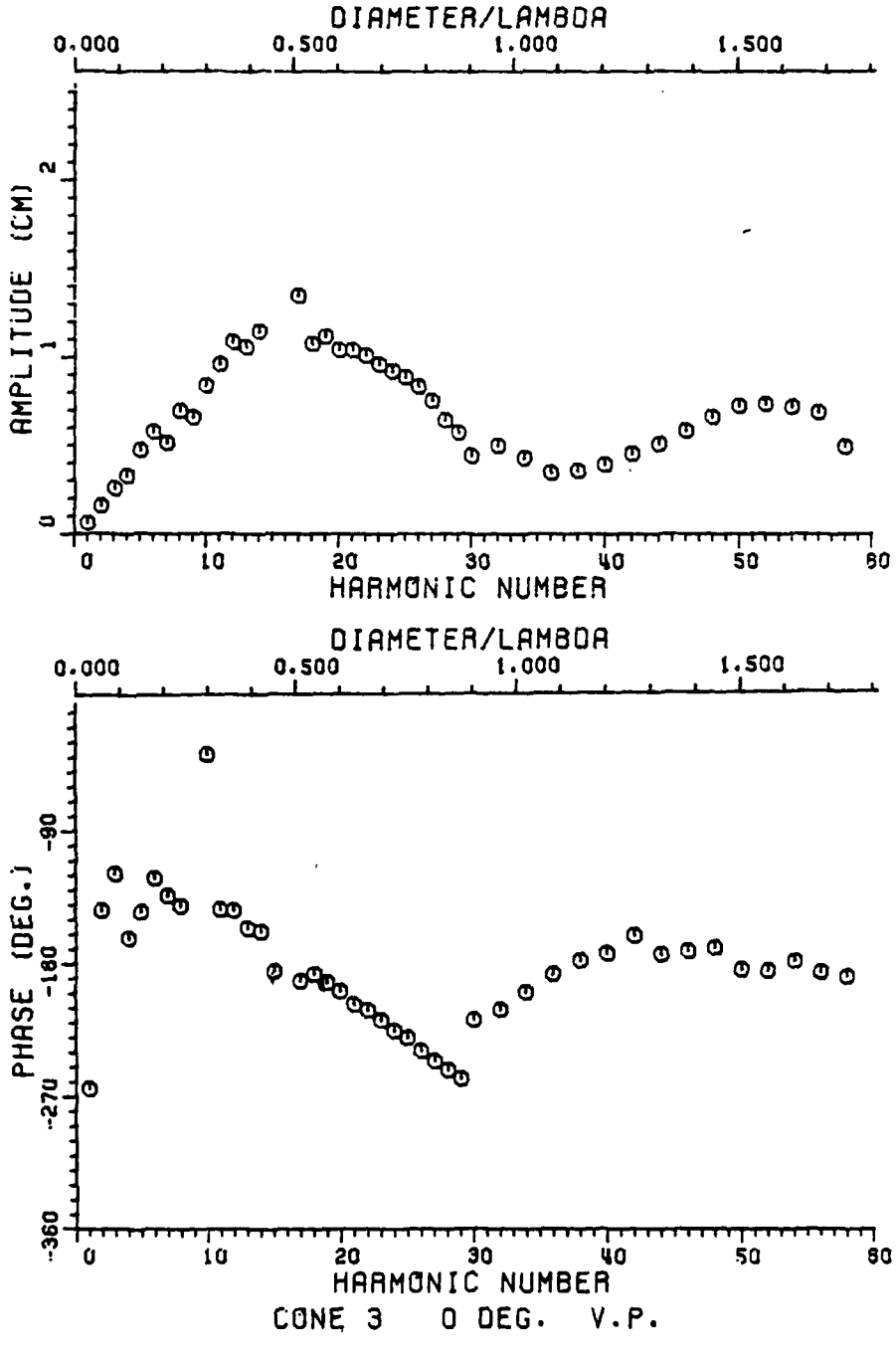

Figure 8. Complex scattering cross-section vs frequency nose-on incidence, Target #3.

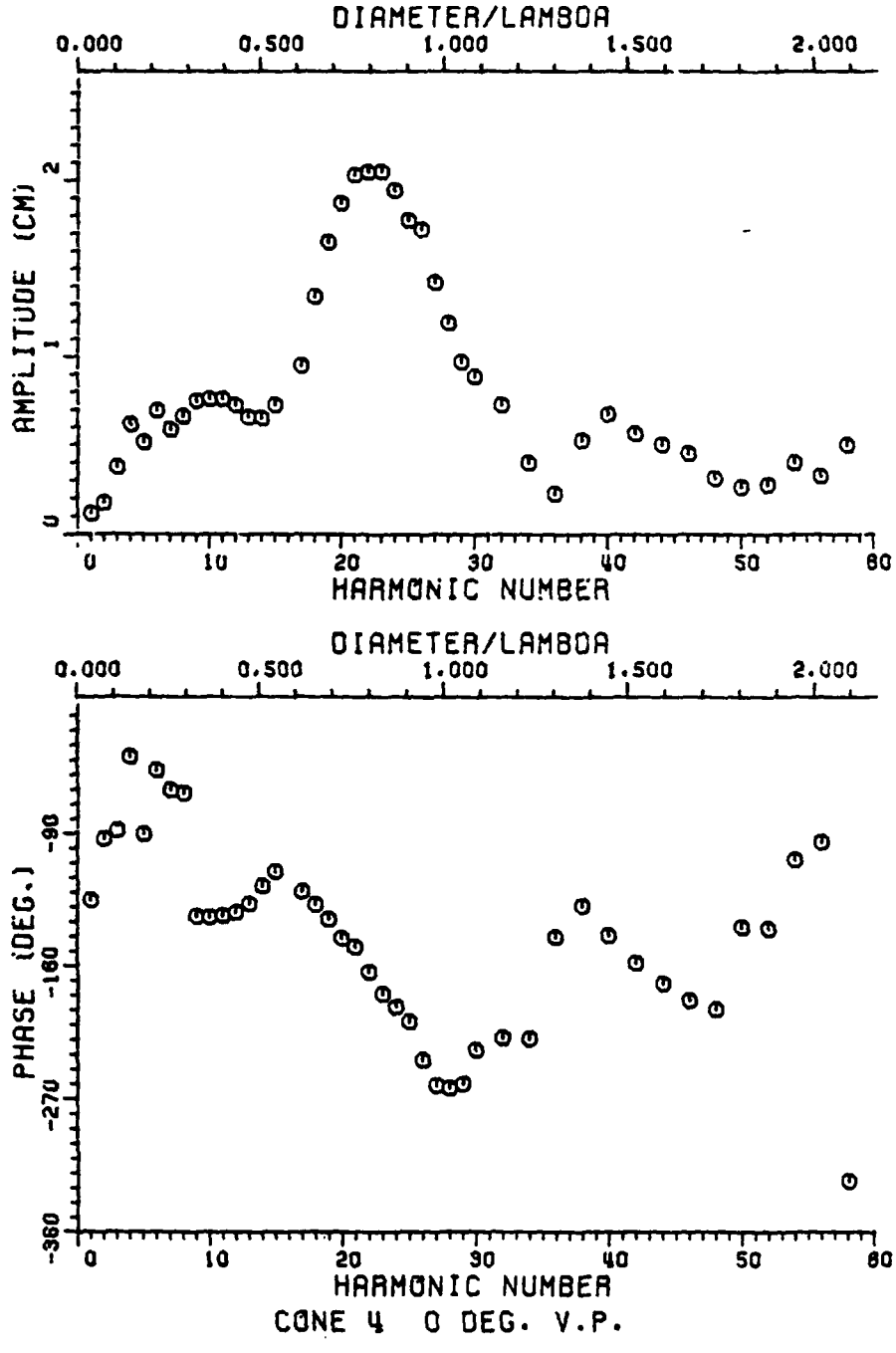

Figure 9. Complex scattering cross-section vs frequency nose-on incidence, Target #4.

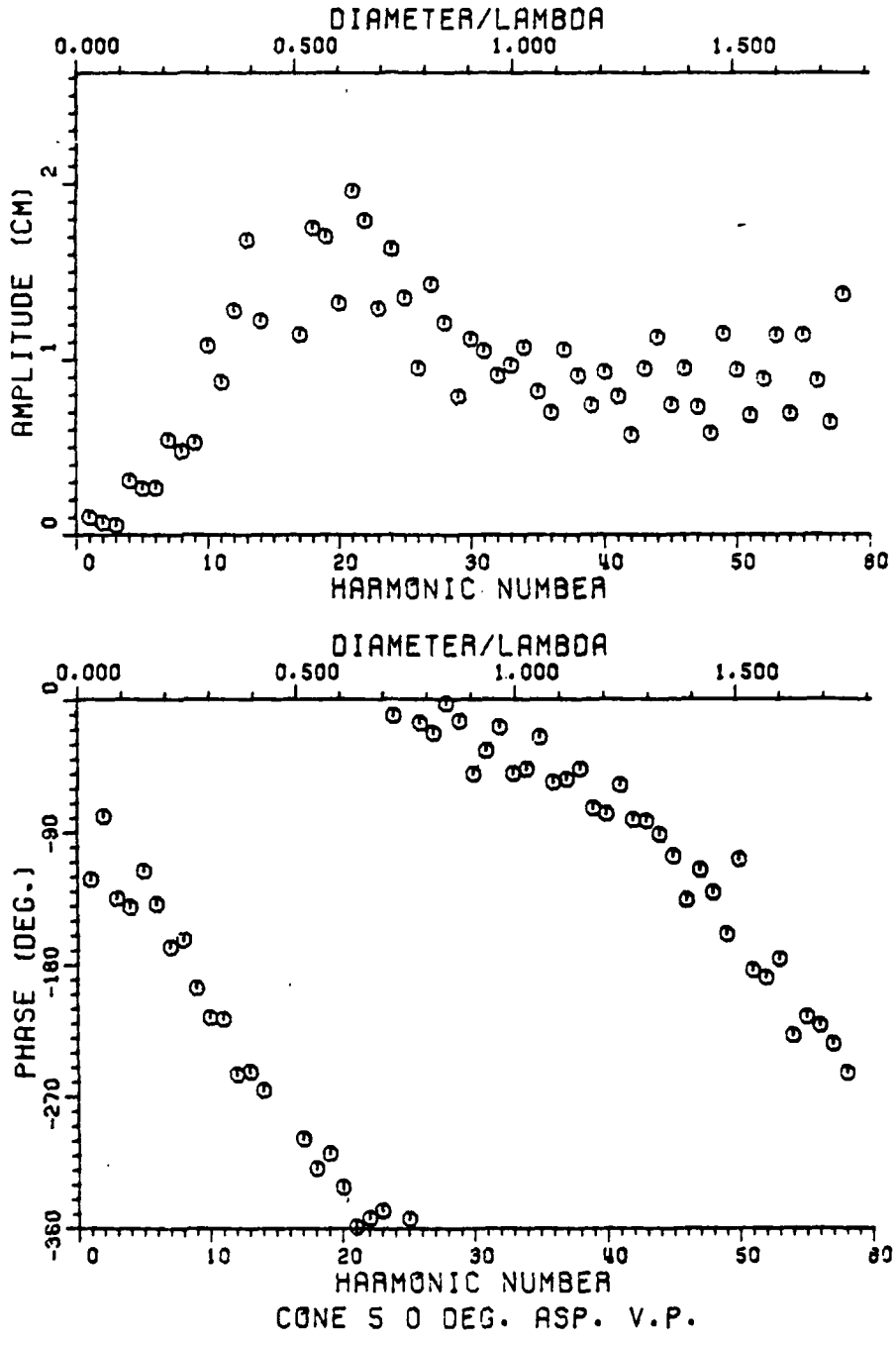

Figure 10. Complex scattering cross-section vs frequency nose-on incidence, Target #5.

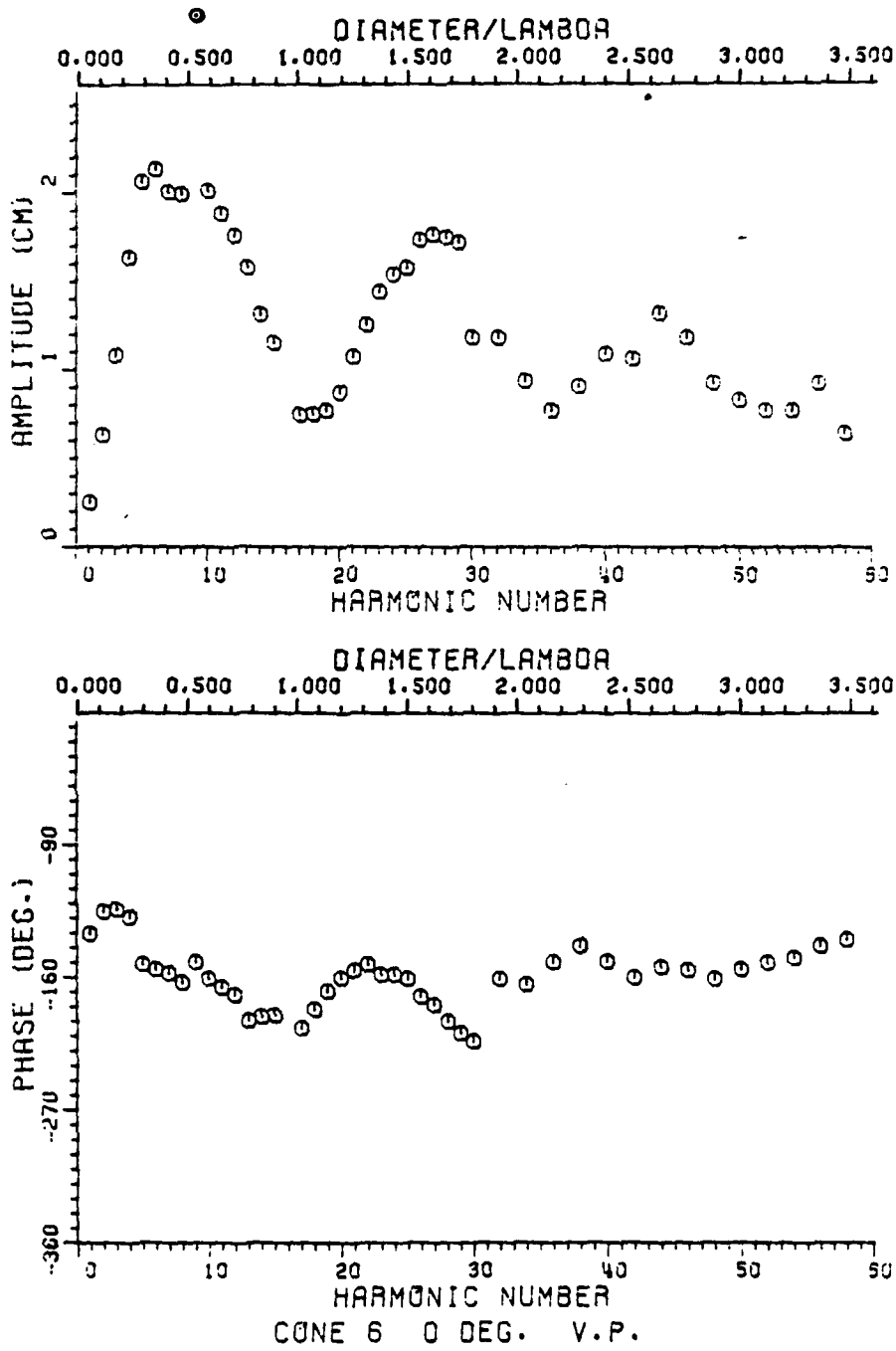

Figure 11. Complex scattering cross-section vs frequency nose-on incidence, Target #6.

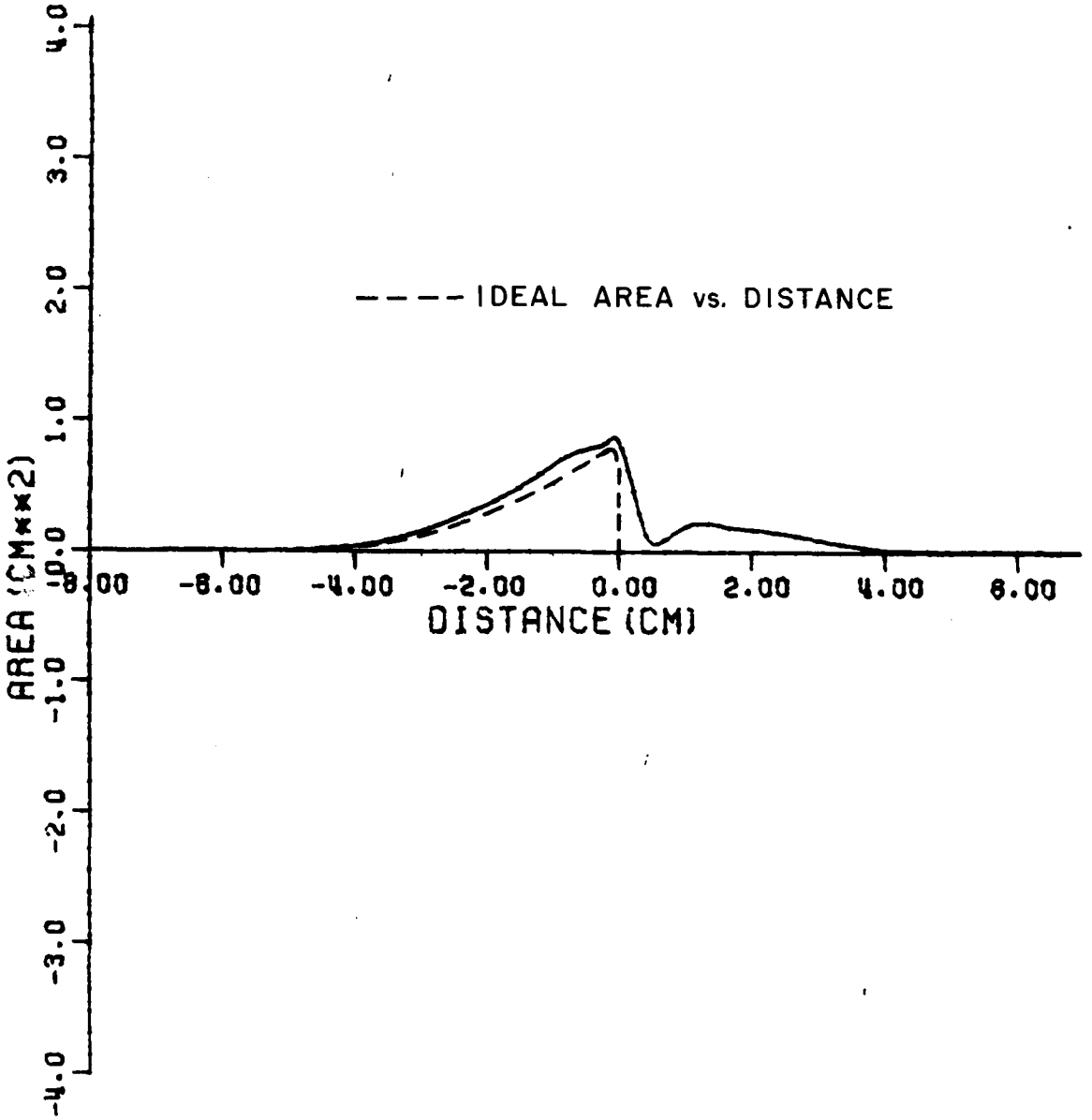

Figure 12. Ramp response waveform, nose-on incidence, Target #1.

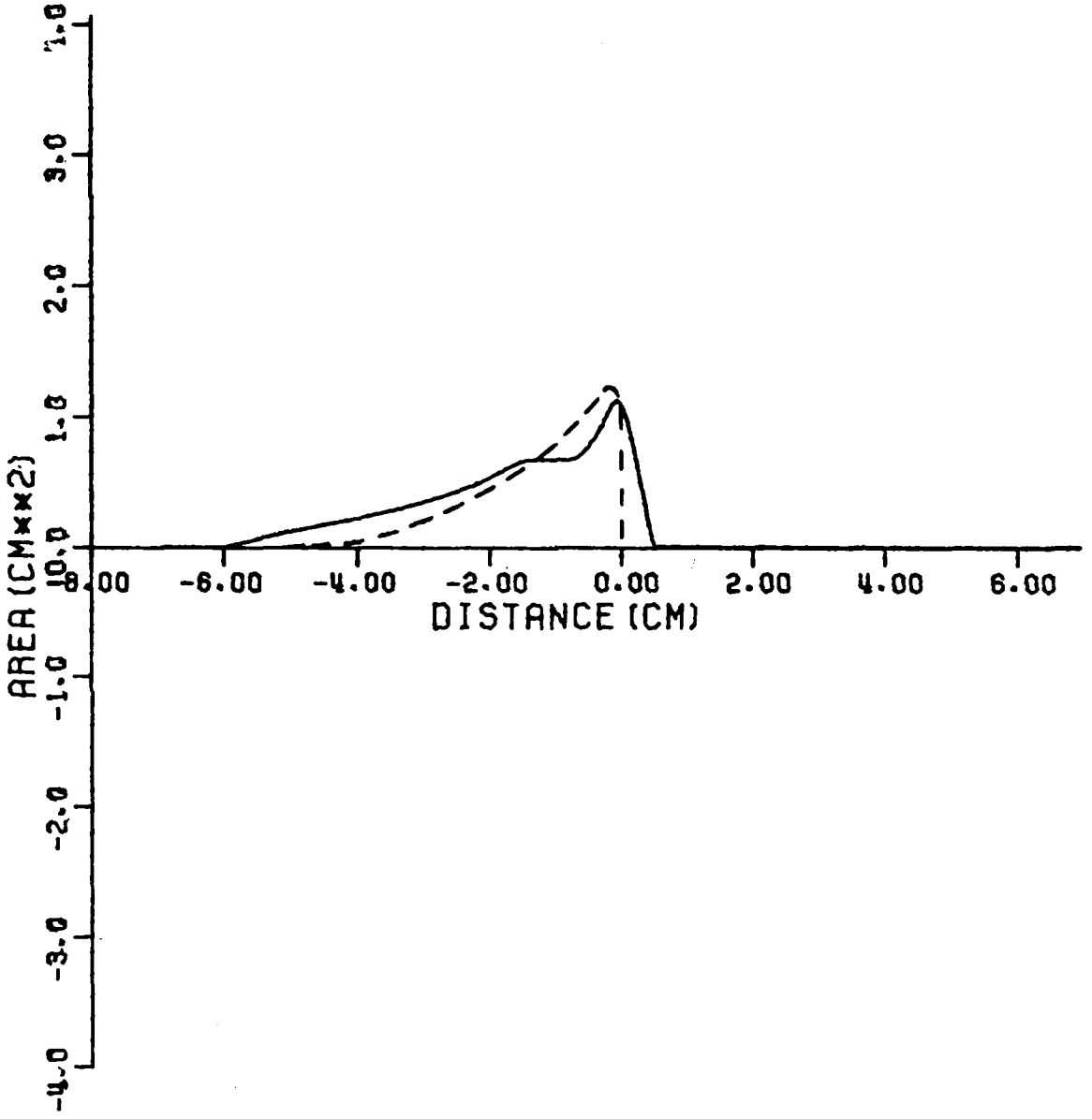

Figure 13. Ramp response waveform, nose-on incidence, Target #2.

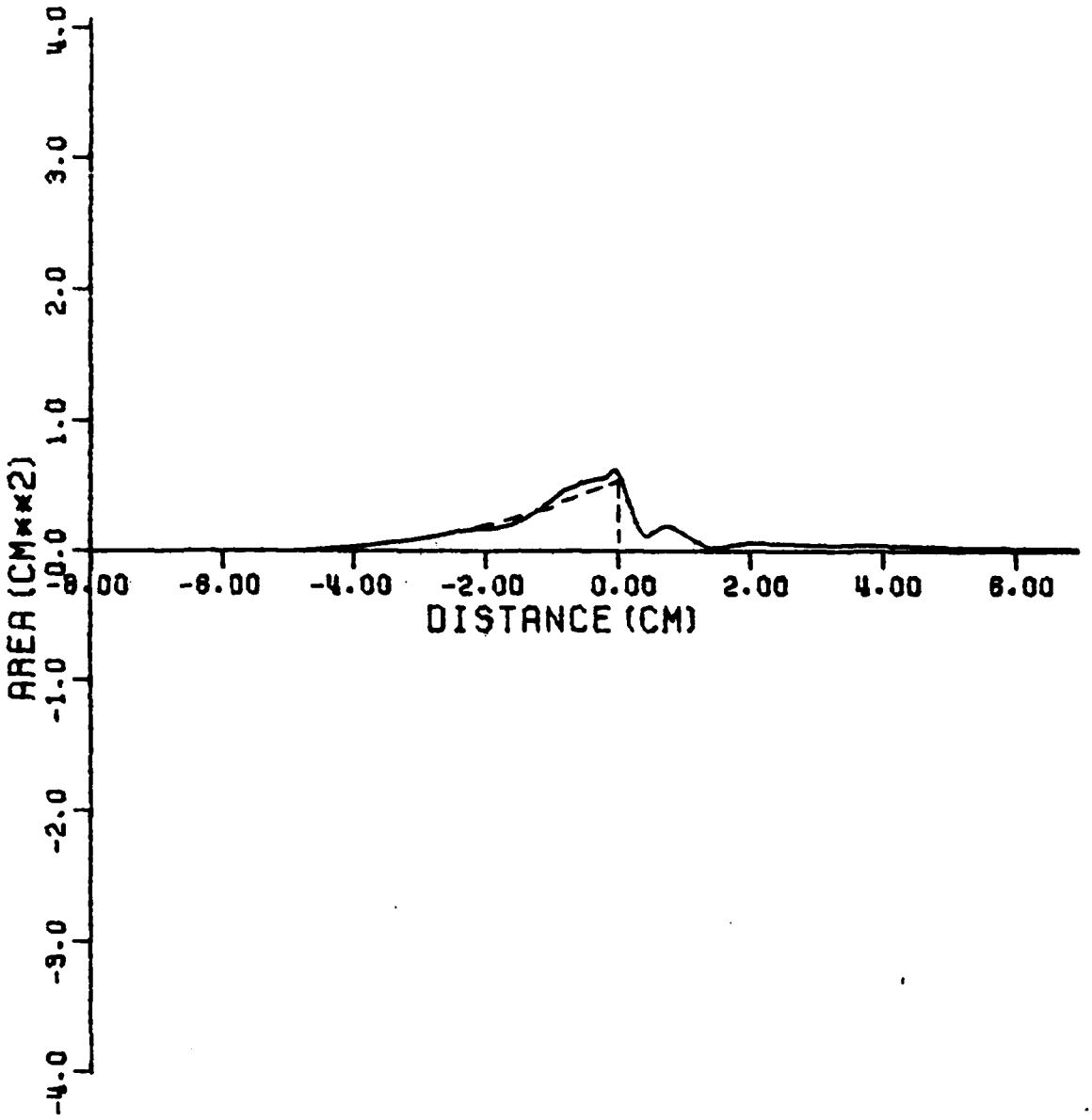

Figure 14. Ramp response waveform, nose-on incidence, Target #3.

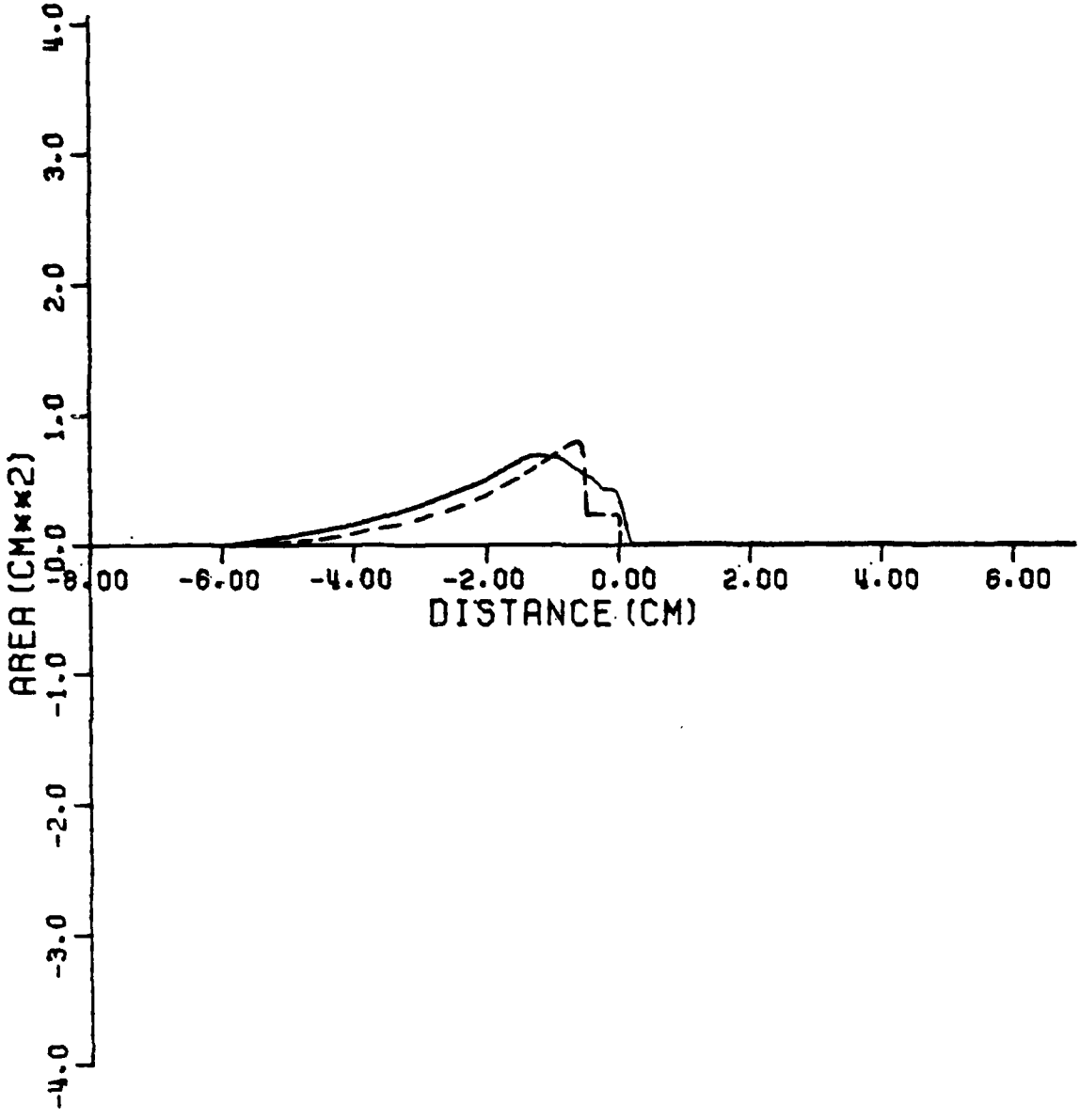

Figure 15. Ramp response waveform, nose-on incidence, Target #4.

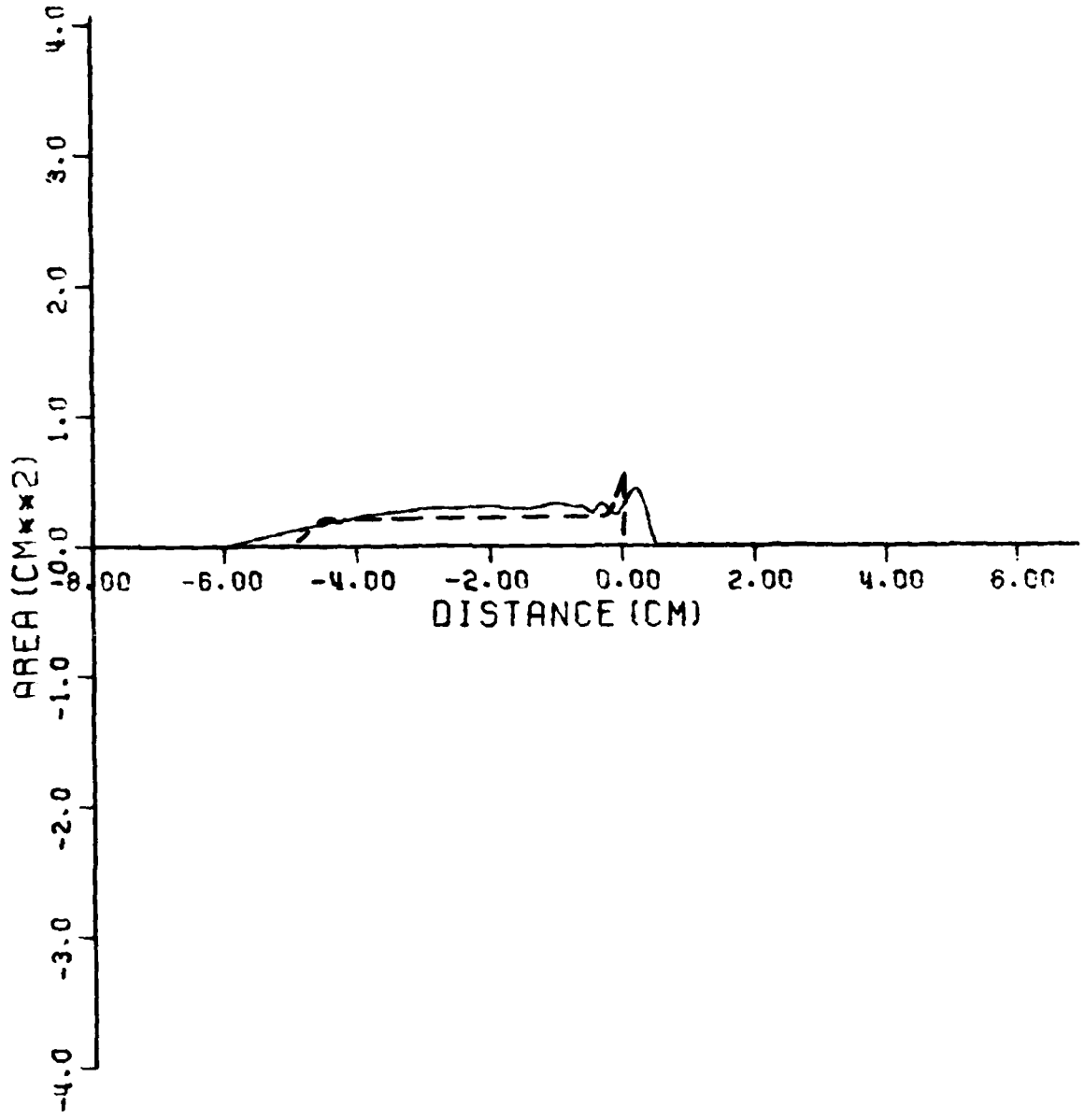

Figure 16. Ramp response waveform, nose-on incidence, Target #5.

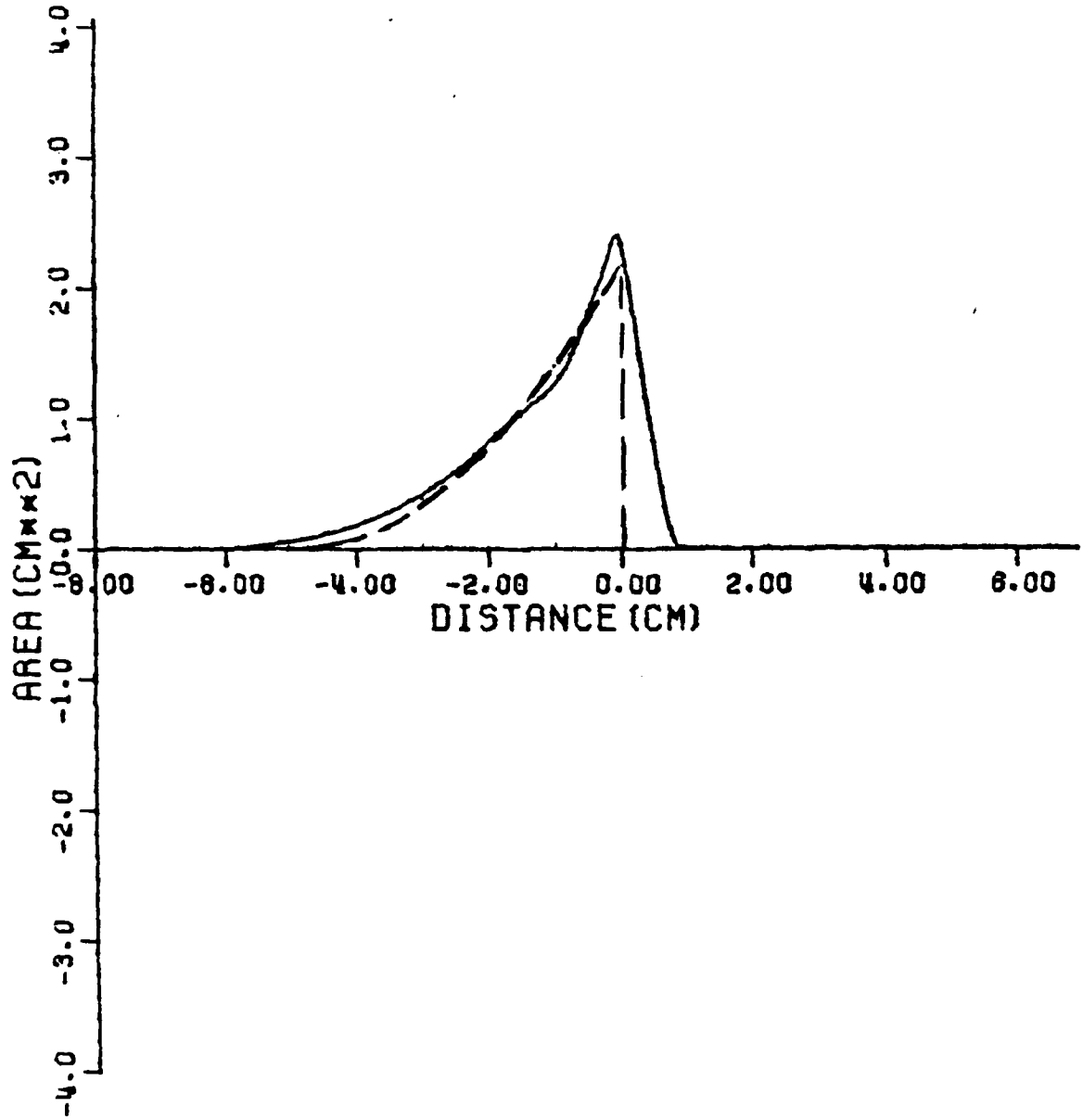

Figure 17. Ramp response waveform, nose-on incidence, Target #6.

III. INVESTIGATION OF LIMITING-SURFACE IMAGING

This technique was first introduced in the early 70's, and demonstrated using 10:1 bandwidth model measurement data on satellite shapes (Reference 9). The goal of this effort was to produce such images for cone-like objects, with two important changes in the data base. First, the frequency spectrum of the transient signature data is at least 30:1. With this greater bandwidth greater resolution of target details might be possible. Second, the range of target look angles was confined to a region within 30^{o} of nose-on, whereas three principle plane look angles had been used before. The amount of image degradation resulting from this restriction needed to be investigated.

A separate technical report, 784785-2, has been written to describe the results of the limiting surface imaging investigation. Images and waveforms are presented, showing the effects of both signature data bandwidth changes and target look angle restrictions. Furthermore, the report describes some important improvements in the imaging algorithm. An automated iteration process has been introduced, so that the imaging is now faster, requiring no operator interaction, and completely objective. The following few paragraphs and figures, abstracted from the technical report, summarize the important results.

A. Characteristics of the Input Data

A set of profile functions derived from measured data were shown in Chapter II, Figures 12 through 17. The plots demonstrate that the measured data does give approximate target cross-section vs distance information for all targets. A discussion in the technical report points out that if discrimination of these targets is desired (rather than identification or imaging) then the targets can be correctly separated using these waveforms alone on the basis of target length (profile function duration), total volume (integration of the profile function) or cone angle (slope of the initial portion of the profile function).

B. Limiting Surface Imaging Process

The basic approach for limiting surface imaging was used here without modification. A limiting surface is constructed for each look angle. The intersection of the multiple limiting surfaces constitute the final three-dimensional image. As before, each limiting surface is an elliptical cylinder whose cross-sectional size along its major axis is set by the profile function. The major axis of each surface, and the length/width ratio and orientation of each slice, are set by "process parameters" which are initially unknown, but must be correctly specified to obtain an occurate image.

An objective criterion of image quality was used in this study. This was a comparison of the cross-sectional area vs distance of the images and the input profile function data for each look angle used. This produces an image volume error estimate. It was shown that for this set of targets, this evaluation technique was satisfactory.

An extensive study was done on the behavior of the images and the image volume error as the process parameters were varied. For example, Figure 18 shows a plot of volume error vs α, one of the process parameters, where target #2 is being imaged using data at 0^{o} (nose-on) and 30^{o} look angles. The parameter α_2 controls the major axis of the limiting surface corresponding to the 30^{o} look angle. It is seen the volume error is minimized when α_2 is at 30^{o}, its correct value.

Figure 19 shows what happens to the limiting surfaces in two cases for the volume error calculation above. When $\alpha_2 = 30^{o}$, it is seen that the two limiting surfaces are lined up, and their intersection (the surface lying within both simultaneously) is a relatively accurate image. However, when $\alpha_2 = 45^{o}$, the two surfaces are not aligned. The image which would be produced in this case is seen in Figure 20. The front tip has been "chopped off" by the misalignment of the two limiting

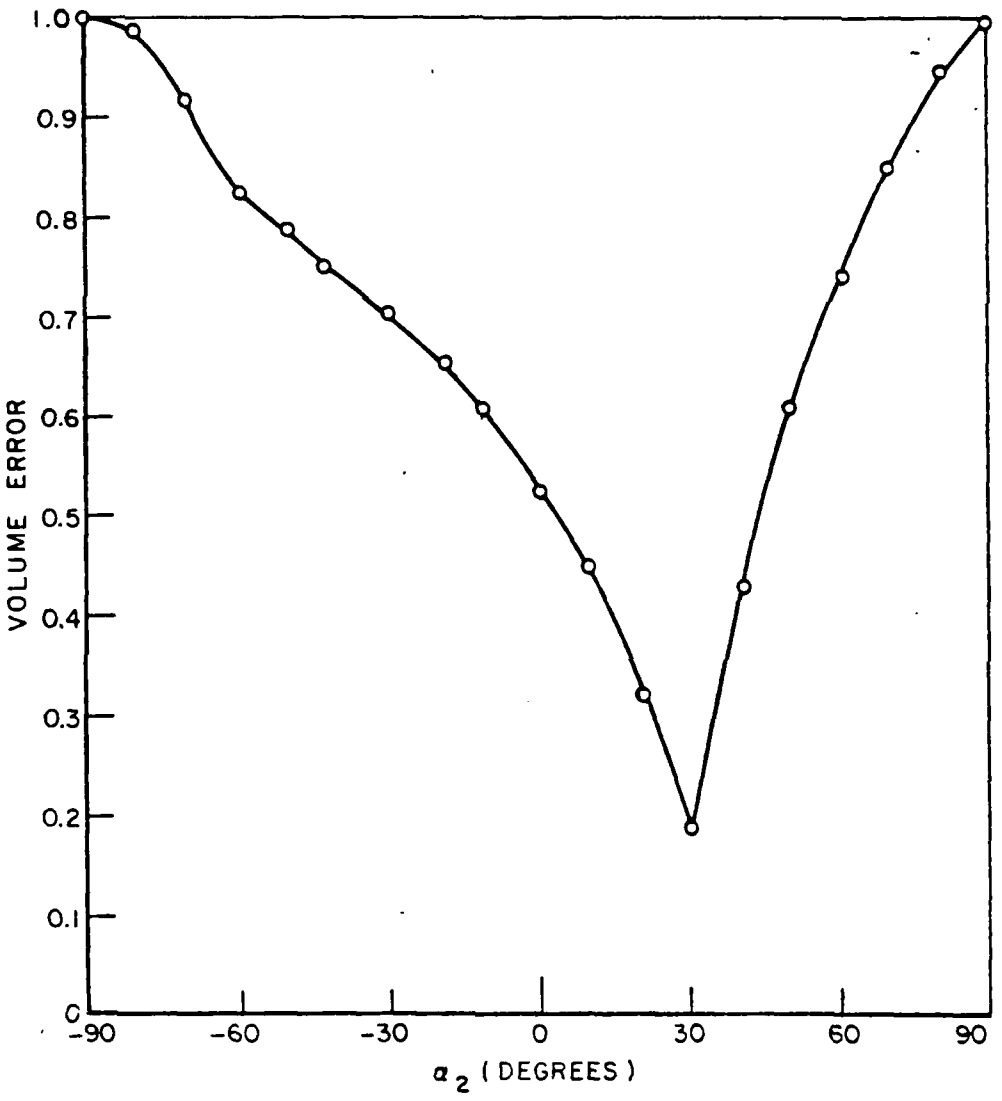

Figure 18. Volume error vs α_2 (a control parameter) for limiting surface imaging of Target #2, 0^0 (nose-on) and 30^0 look angles.

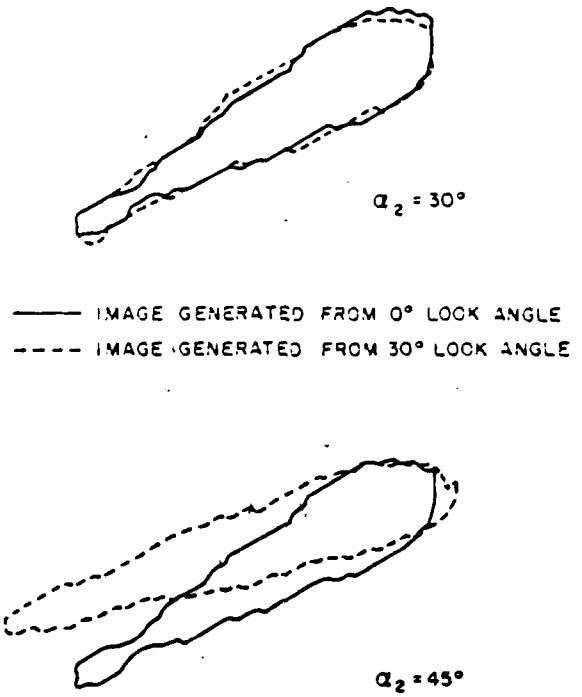

Figure 19. Example of imaging dependence on α_2.

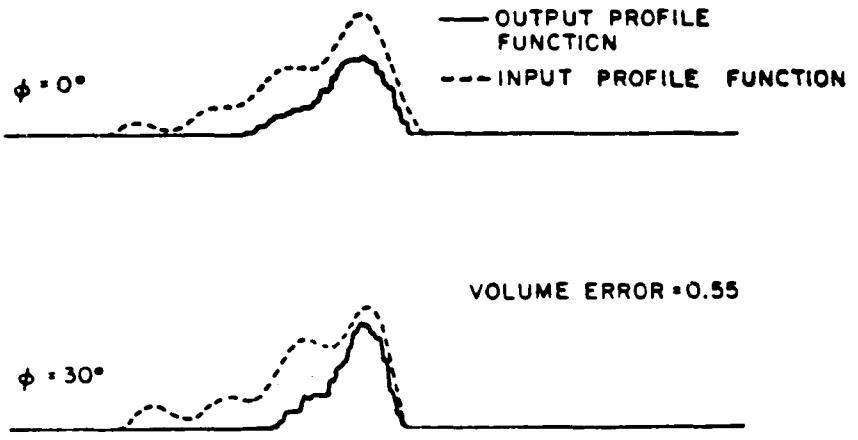

Figure 20. Image of target 2 with $\alpha_2 = 45^0$ (incorrect value) and resulting profile functions.

surfaces. The profile functions in Figure 20 show how this effect also produces a volume error.

C. Automated Imaging

A study of the volume error vs all process control parameter variations revealed that the process if relatively "well behaved", i.e., incorrect values of each parameter give measurable increases in the volume error, and volume error increases proportional to process parameter error. Because of this characteristic, an automated iteration procedure was developed to obtain the image, and was evaluated using several specific test cases.

The procedure which was used is a linear direct search method. A linear method is one which uses a set of direction vectors, in this case the parameter coordinate axes, throughout the search. A direct search method is any minimization technique not requiring explicit evaluation of any derivatives of the function being minimized. The procedure begins by determining at some initial point which direction along each parameter one would have to travel in order for volume error to decrease. This is done by making small perturbations from the initial point along each parameter direction. Each parameter is then incremented by some fixed amount in the appropriate direction. This is equivalent to moving only roughly in the direction of the gradient. The elliptical cross section aspect ratio is actually incremented logarithmically because of the nature of this parameter. This procedure is repeated until the vicinity of the minimum has been located. The process converges to the minimum by decreasing the increment sizes each time the minimum is passed as explained above.

The possible initial limiting surface parameter combinations can be represented by several cases. These cases demonstrate the performance and restrictions of the iterative algorithm. The ideal 0^{o} and 30^{o} profile functions for target 6 will be used in each example unless

otherwise indicated. The first case is when the limiting surface parameters are known for one look angle and unknown for the other. The algorithm will iterate to very nearly the correct values of the unknown parameters. For example, with the parameters for the 0^o look angle correct and the initial 30^o look angle parameters set at $\alpha_2 = 60^o$, $\beta_2 = 140^o$, $\beta_2 = 50^o$, and $R_2 = 0.5$, the resulting parameter values are $\alpha_2 = 29.5$, $\beta_2 = 179.7$, $\gamma_2 = -0.25$ and $R_2 = 1.19$. This example required 20 iterations with the initial parameter increments set at 4.9^o, 4.9^o, 20.1^o and 0.0792 for α_2, β_2, γ_2, and R_2, respectively. Volume error decreased from 0.77 initially to 0.186. This example was repeated using the measured 0^o, 29-harmonic ramp response and 30^o, 10-harmonic response for target 6. This time 18 iterations were required and the resulting parameter values were $\alpha_2 = 29.38$, $\beta_2 = 179.51$, $\gamma_2 = -9.67$, and $R_2 = 1.083$. The final image and image profile functions are shown in Figure 21. Here the volume error decreases from 0.729 to 0.164.

Performance is less satisfactory when parameters for both look angles are unknown. When α and R for both look angles are unknown, the algorithm iterates to a point where the aspect ratios are approximately equal and the elliptical cross sections have approximately the same tilt. In this case the volume error decreased from 0.697 to 0.193. The final image is significantly distorted although the volume error is nearly the same as for a correct image. The problem here is that the correct aspect ratios for the 0^o and 30^o look angles are nearly equal (1.0, 1.16). Apparently any combination of nearly equal aspect ratios will result in good agreement between the actual and image profile functions. It is expected that if a second look angle closer to broadside was used so that the aspect ratios for the two look angles differed by a significant amount, then better iteration to the correct aspect ratio values might result. This example illustrates that volume error is not always a good indicator of image accuracy.

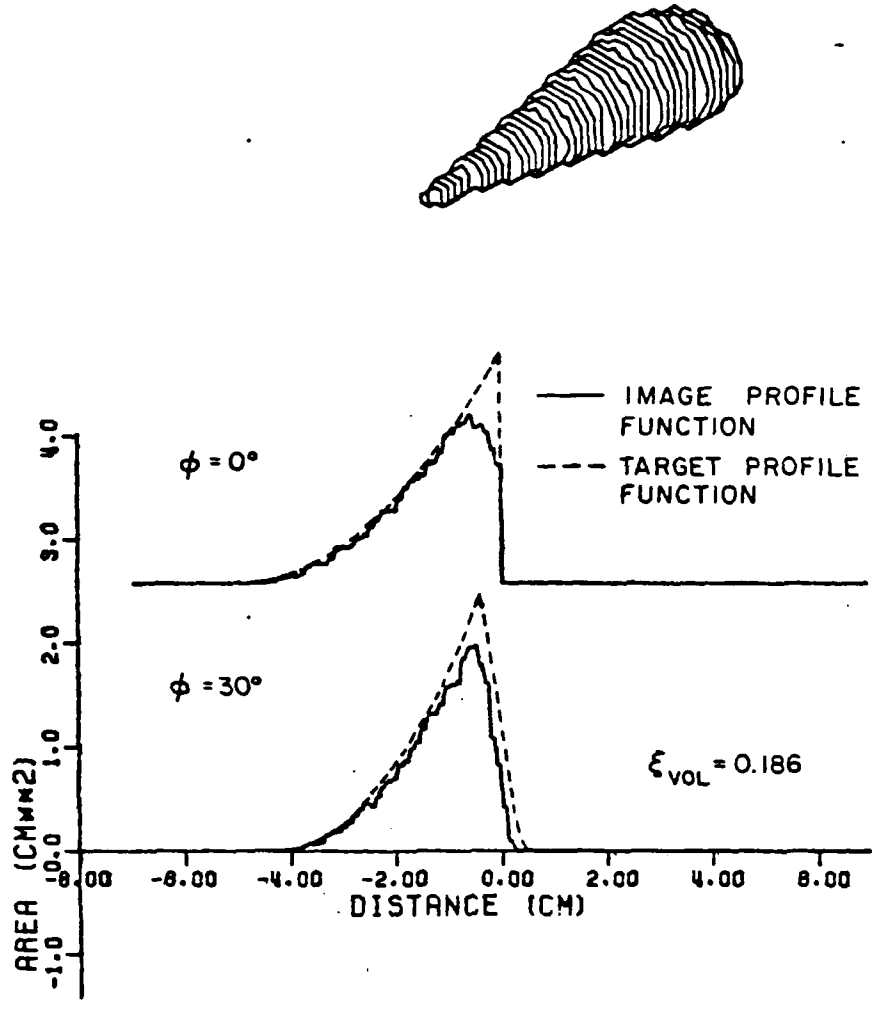

Figure 21. Final image and profile functions for iterative imaging, Target #6.

Summary

The goal of the limiting surface imaging study was to examine its capabilities for cone targets using severely limited input data, and to eliminate the need for a priori knowledge for determining process control parameters' values.

Image volume error was defined and shown to correspond to image accuracy, i.e., the agreement between a target and its image. In particular, volume error was observed as a function of the various limiting surface parameters. For a cone target it was demonstrated that volume error was minimized as the limiting surface parameters approached their correct values. In addition it was shown that in certain cases, volume error decreased monotonically towards the correct parameter values. An algorithm based upon minimizing volume error was developed for iterating to the correct limiting surface parameter values. The algorithm was shown to iterate correctly in several cases when data corresponding to a cone target is used. Specifically, it was shown that the angles specifying the elliptical cross section center lines could be correctly determined. It was also shown that if the limiting surface parameters were known for one look angle and unknown for another, then the unknown parameters could be determined.

In the imaging examples studied, backscatter data at only two aspects were used. In addition, the look angles were separated by only 30^{o}. This was done to approximate a practical system. However, the resulting ramp response from the two look angles contain largely overlapping information. Only ramp responses obtained from mutually-orthogonal look angles contain totally independent information. The result of using only a few look angles separated by a relatively small angular distance is that the ramp responses obtained do not uniquely define the target. For instance, the 0^{o} and 30^{o} aspect profile functions for a 3:1 right-circular cone (target 6) were shown to correspond almost nearly as well to a flattened cone. The volume errors for the correct

image and the flattened image were nearly equal. The use of a greater number of look angles separated by a larger angular distance would reduce the chance of a set of ramp responses corresponding to more than one object and would increase the probability of correct parameter determination.

Several secondary goals were also accomplished in this study. Ten-harmonic ramp responses, for a set of cone and cone-cylinder targets were measured and the results presented. An automated method for processing ramp response waveforms to approximate the target profile functions was also presented. It was demonstrated that most of the targets could be discriminated from characteristics which were determined directly from the ramp responses. Images using measured and corrected ramp responses and calculated limiting surface parameter values were generated for each target. The images were seen to be representative of their corresponding targets although lacking in sharp details.

IV. HIGH FREQUENCY IMAGING

An important part of this research effort was the study of the application and interpretation of "high-frequency" imaging or inverse scattering techniques for cone targets, using the limited range of look angles permitted. It was decided early in the program to concentrate on physical optics inverse scattering techniques, an area where much has been written. In applying the physical optics approach to this specific application, some new insight and new results were obtained, and these are contained in a separate technical report (784785-4). This chapter abstracts a few portions of that report.

The Bojarski Identity

In a series of reports Norbert Bojarski (References 15-19) has formulated a relationship between the monostatic scattered far field cross section of perfect conductors and the geometry of the conductors. The results are based on the physical optics approximation.

If the scatterer is expressed in three dimensions by its characteristic function $\gamma(\bar{x})$ where,

$$\gamma(\bar{x}) = \begin{cases} 1 & \text{inside the body} \\ 0 & \text{outside the body} \end{cases} \tag{17}$$

and if the scattered far field cross section $\rho(\bar{p})$ is used to define $\Gamma(\bar{p})$ where,

$$\Gamma(\bar{p}) = 4\pi \frac{\rho(\bar{p}) + \rho^*(-\bar{p})}{|p|^2} \tag{18}$$

with $\rho(\bar{p})$ = the field cross section

$$\bar{p} = \frac{2\omega}{c}\bar{a} = 2\bar{k} \left(\frac{\text{cycles}}{\text{meter}}\right)$$

$\bar{k}$ = wavenumber propagation vector in the direction of aspect:

then Bojarski has shown that

$$\gamma(\bar{x}) = \frac{1}{(2\pi)^3} \int_{-\infty}^{\infty} \Gamma(\bar{p})\, e^{i\bar{p}\cdot\bar{x}}\, d^3\bar{x} \tag{19}$$

This technique is normally considered to be a high frequency one because:

1. The relationship is independent of incident field polarization.

2. No reverberation of energy on the target structure is accounted for.

3. Excitation of the shadowed side of the body for a particular angle of incidence $\bar{p}$ is assumed to be zero.

The correspondence between measured data for the cone targets and predicted scattering using both physical optics inverse scattering and the Bojarski transform was studied. The measured data include both low frequencies and high frequencies. The frequency-domain data for the square root of the scattering cross-section of the nose-on look angle for target #6, a 3:1 cone, are shown in Figure 22. Time-domain ramp response and step response waveforms corresponding to the data of Figure 22 are shown in Figures 23 and 24 respectively.

As seen in the frequency spectra, the two-sided Bojarski analysis agrees best with measured data for the first 7 harmonics, then the predictions of both analytical approaches depart substantially from the measured results. The ramp response plots give more insight into the discrepancies. It is seen that both analysis approaches give identical and quite accurate, predictions for the forward region of the cone. However, neither technique gives an accurate picture of the scattering mechanisms associated with the back edge. This problem is also discussed in the report on measured data, where it is pointed out that other analysis techniques exist for correctly predicting these effects. The step response plots also show general agreement in the forward region, but differences near the rear edge.

It is thus concluded that the two-sided physical optics approximation is good for low frequency scattering predictions on cone targets near nose-on, and that both physical optics analysis methods correctly predict the scattering from the forward portion of the cone. However, the techniques are seen to be inaccurate for high frequencies at look angles where diffraction mechanisms contribute significantly to an object's total scattering cross-section.

Regardless of the accuracy of the physical optics approximation, the data used in this effort (angles less than 30^{0} from nose-on) comprise only a subset of the complete characteristic function in $\bar{p}$ space. The effect of this "windowing" was examined. Figure 25 shows a set of 2-dimensional shapes, whose ideal characteristic functions in $\bar{p}$ space

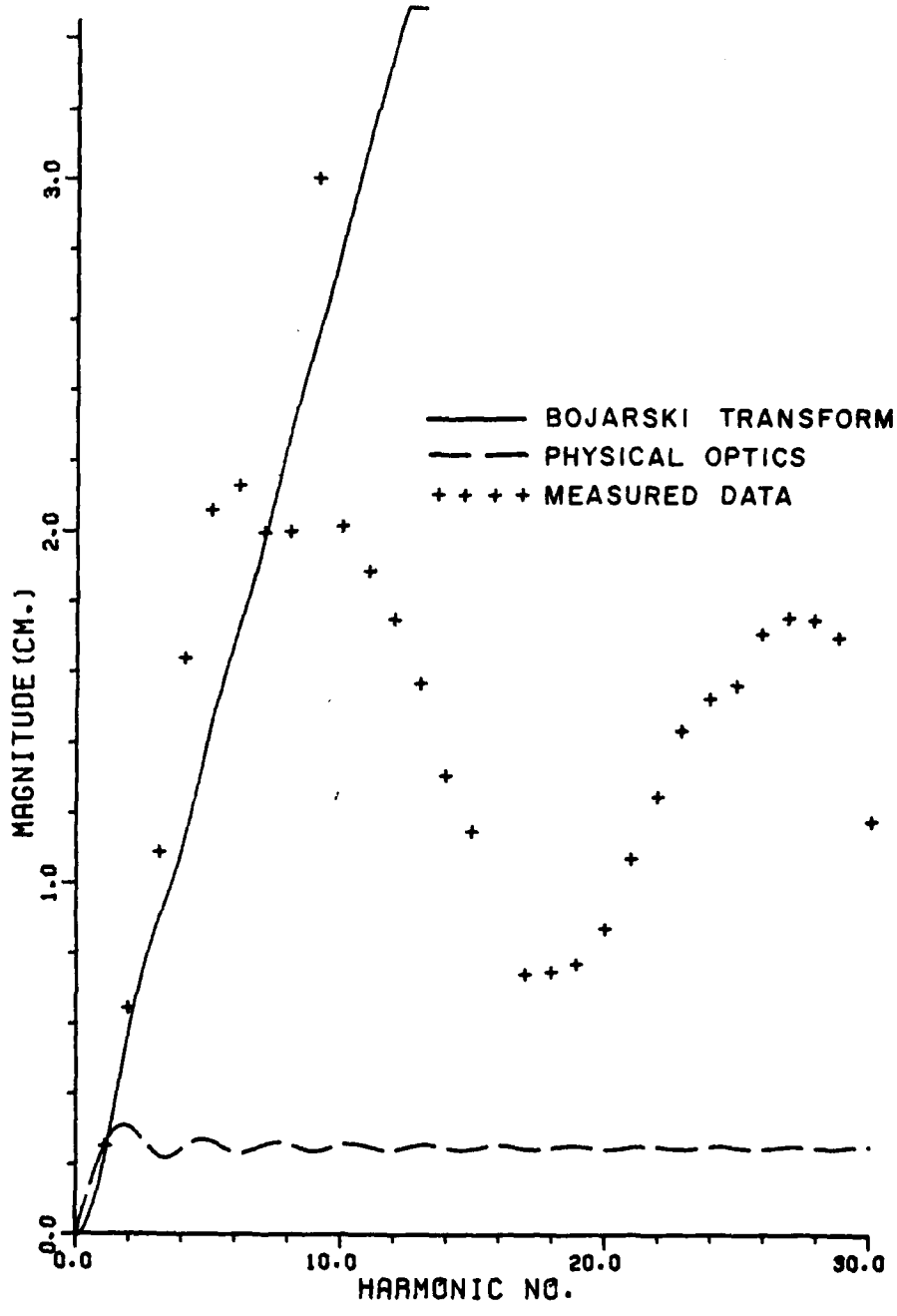

Figure 22. Frequency-domain scattering, physical optics calculations vs measured data, Target 6.

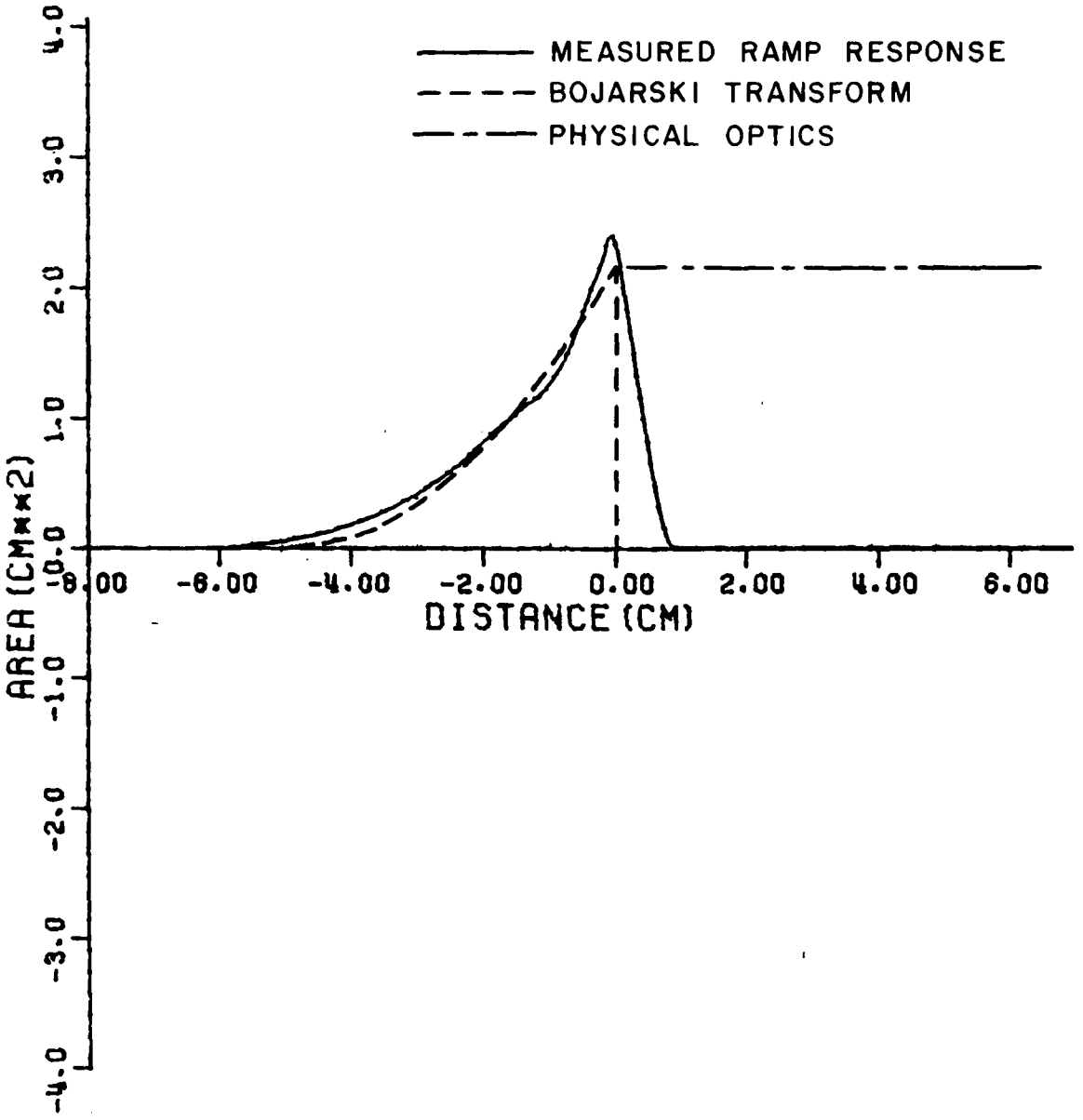

Figure 23. Ramp response waveforms, physical optics calculations vs measured data, Target 6.

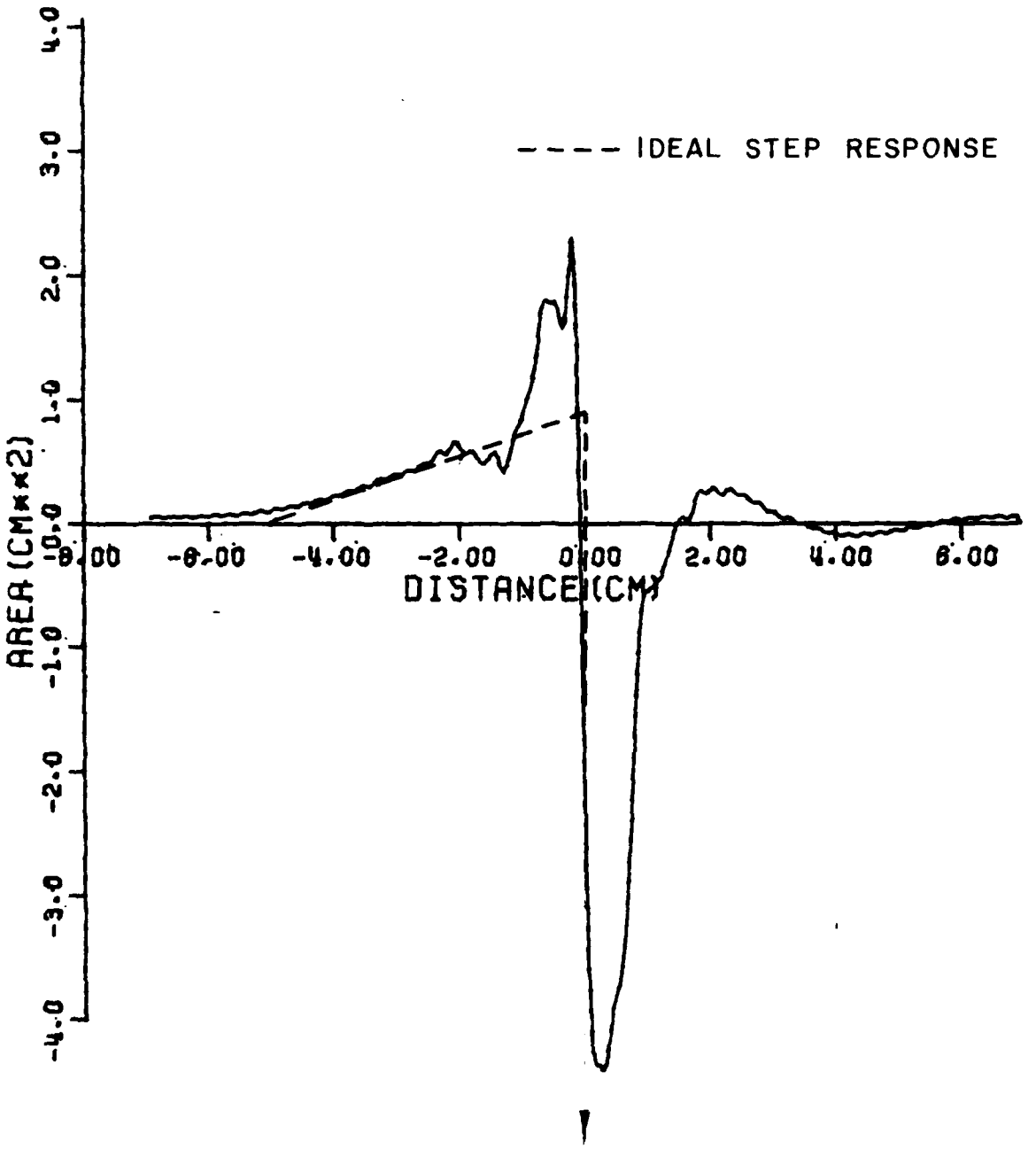

Figure 24. Step response waveforms, physical optics calculations vs measured data, Target 6.

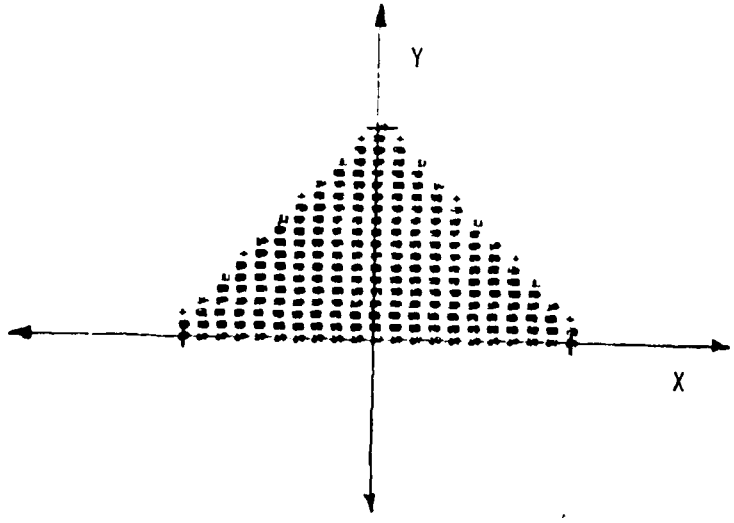

a. triangle

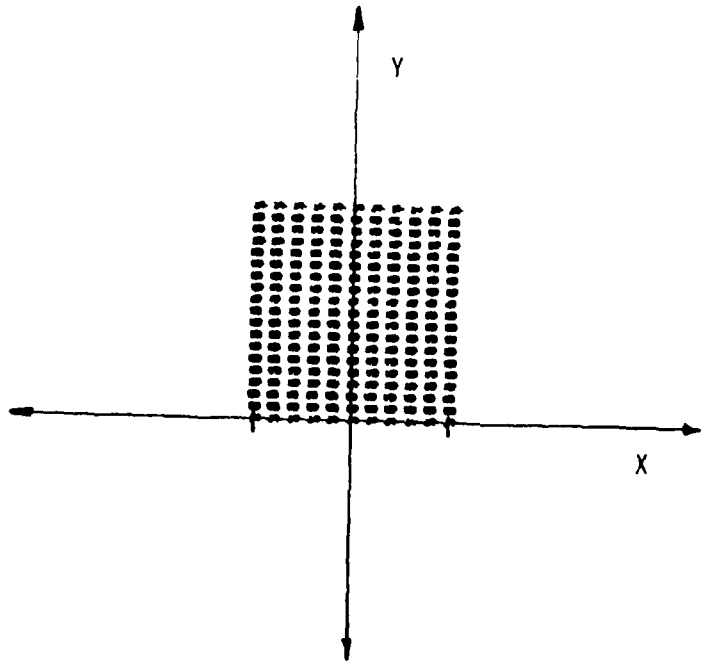

b. square

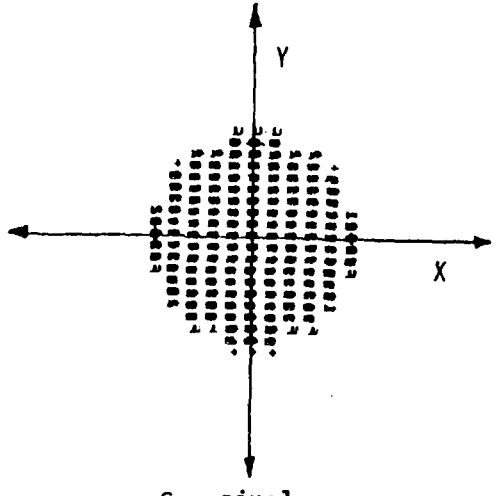

c. circle

Figure 25. Two-dimensional shapes for windowing analysis computed grey-scale plot.

were calculated. For example, the magnitude of $\Gamma(\bar{p})$ for the triangle is shown in Figure 26. Next, angular windowing was done on the characteristic functions. Windowing angles of 60^{o} and 30^{o} from nose on were tried, and the resulting images are plotted in Figures 27 and 28, respectively. It is seen when look angles perpendicular to all edges are not included, then the image becomes degraded to a great extent.

Following the study of windowing, our effort at direct image generation using the measured data and physical optics inverse diffraction techniques was redirected toward a quasi-identification approach; i.e., if it is known that an object is cone-like, and if broadband scattering data over a $\pm 30^{o}$ range of look angles with respect to nose-on is obtained, then what techniques for determining important characteristics such as size (length, base-diameter) and shape (sharp edges, cone angles) can be discovered using physical optics inverse scattering concepts.

One important result of the target characteristic investigation is that the base diameter of the cone can be inferred from the slope of the frequency-domain signature data at low frequencies. Further study of the correspondence between the target length and/or target cone angle vs signature properties showed that this is definitely a second order effect compared to base diameter for near-nose-on data. However, the technical report contains a discussion of a relationship between high-frequency scattering vs angle and cone length.

V. INVESTIGATION OF IMAGING FROM LASER-EXCITED TRANSIENT RESPONSES

At this Laboratory there is another research effort funded by the Ballistic Missile Defense Division which is concerned with the excitation of electromagnetic transient response signatures by laser pulses incident on a conducting target. Depending upon the efficiency of this excitation, and its characteristics vs target material, target shape, and laser parameters, this might be a feasible technique for applying the target imaging process to distant targets. What is envisioned is

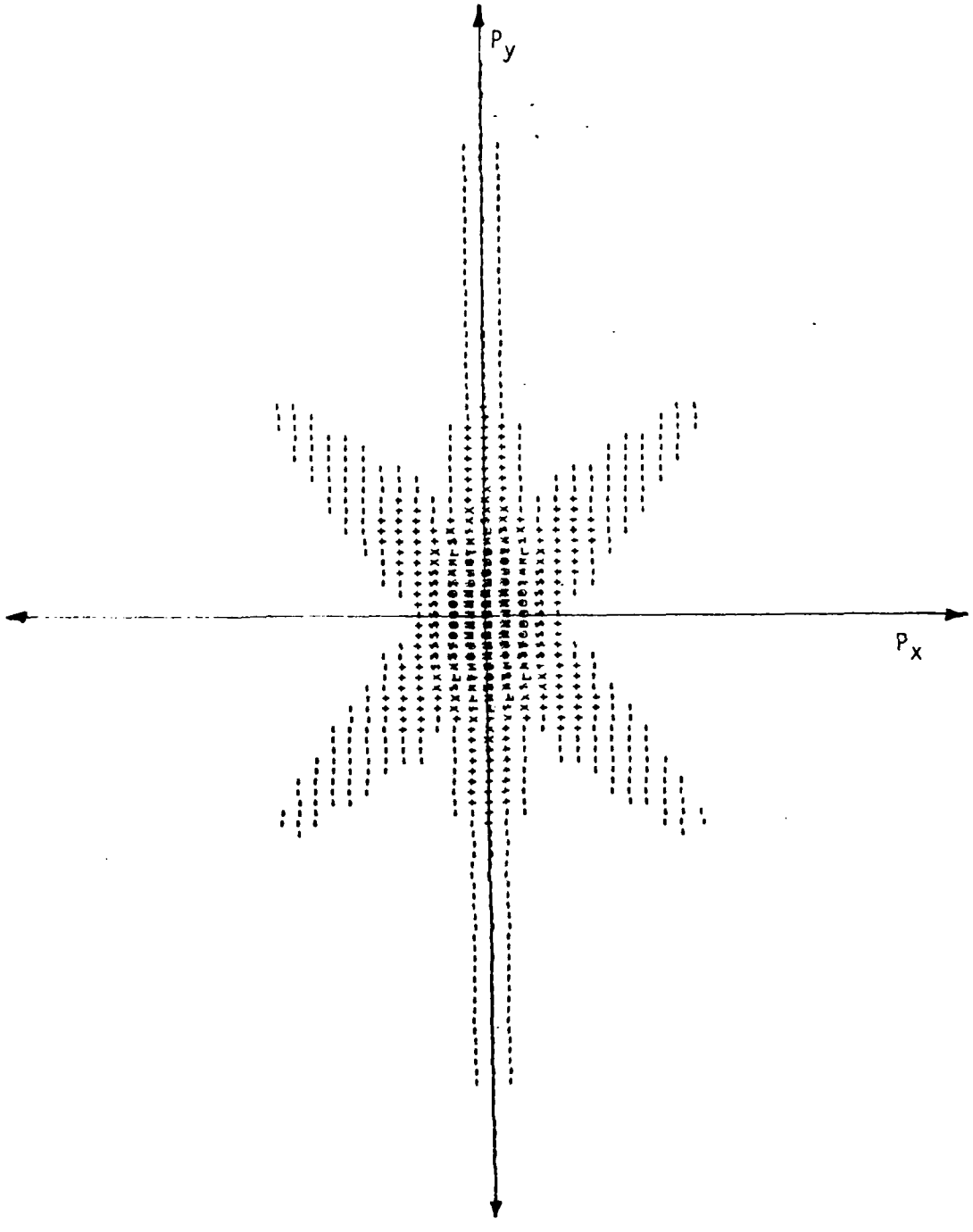

Figure 26. Two-dimensional scattered field magnitude for triangle, computed grey-scale plot.

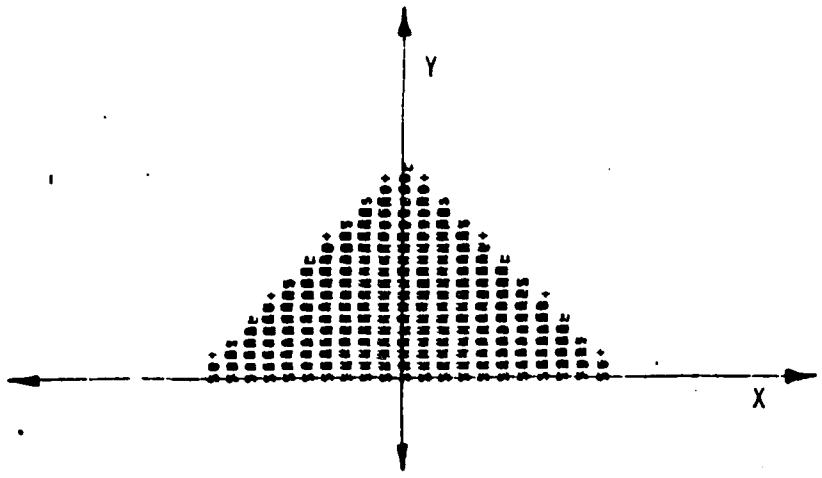

a. triangle

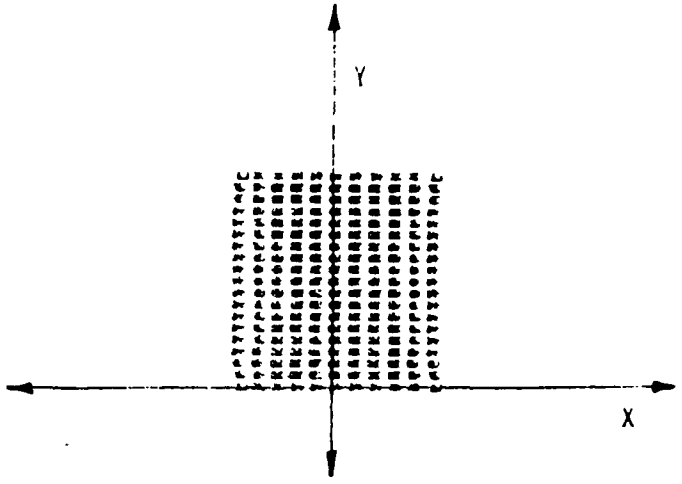

b. square

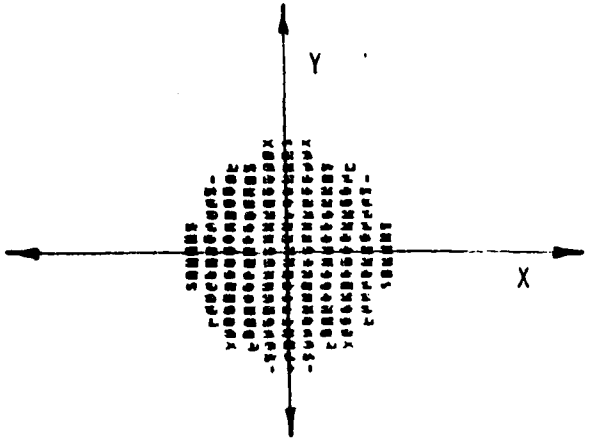

c. circle

Figure 27. Images after 60^{o} aspect angle and threshold filtering, computed grey-scale plots.

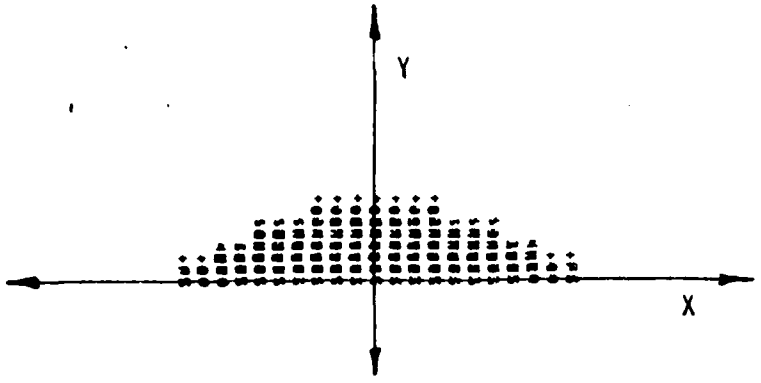

a. triangle=

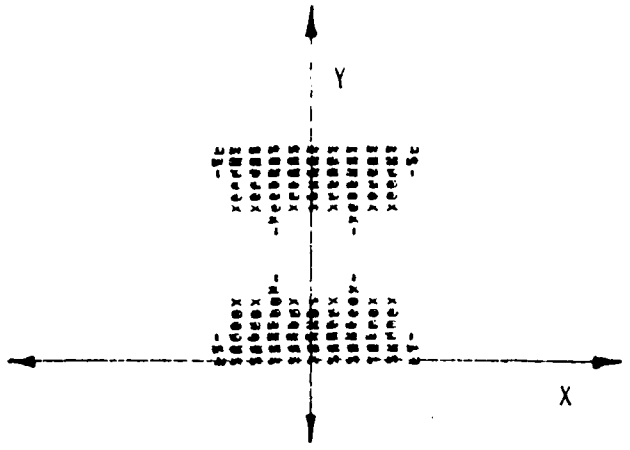

b. square

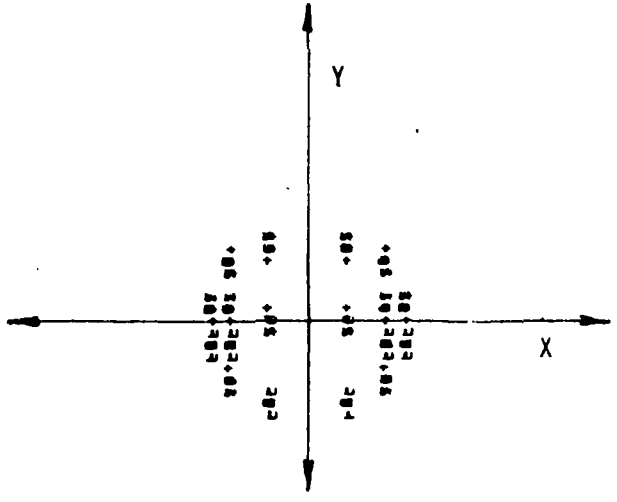

c. circle

Figure 28. Images after 30^{o} aspect angle and threshold filtering, computed grey-scale plots.

the use of a high-powered laser to illuminate a target, producing an electromagnetic transient response which is received with broadband radar equipment. The transient response produced this way can contain low-frequency components (1 to 100 MHz) which would be difficult to produce with a radar transmitter. (For example, the radar operating at 1 MHz with the required 1^{o} transmitting antenna beamwidth would require an antenna aperture of $2.94 \cdot 10^{8}$ m^2.)

An experimental apparatus has been constructed in order to verify the existence of the excitation, and to examine the efficiency of the non-linear process, and its dependence on signal strength and target material (Report 4786-1). With this experiment, a small $\approx 1/2$ mm^2 spot can be illuminated with sufficient intensity to repeatibly produce the effect. It appears that the spot behaves like a small monopole, which produces an impulsive signal whose duration is approximately 1 nsec.

Some tests of target identification have been performed. For example, the transient response for a thin wire, excited at the tip by the laser pulse, is shown in Figure 29. The calculated response assuming an electromagnetic pulse excitation at the same point is shown in Figure 30. The two waveforms are in very good agreement. Furthermore, the frequency of the reverberations and their decay rate are characteristic of the wire length and diameter. Thus, these waveforms demonstrate that target identification is feasible using laser excitation of an electromagnetic transient response. If the final estimates of conversion efficiency look promising, then it should be possible to combine the laser excitation work with several efforts concentrating on target identification from transient response signatures (Reference 20) to produce a new technique for target identification.

However the emphasis of this research contract is on target <u>imaging</u> from transient scattering. As was previously discussed, the images are based on the properties of the initial portion of the time-domain ramp response signature (before the reverberations actually begin),

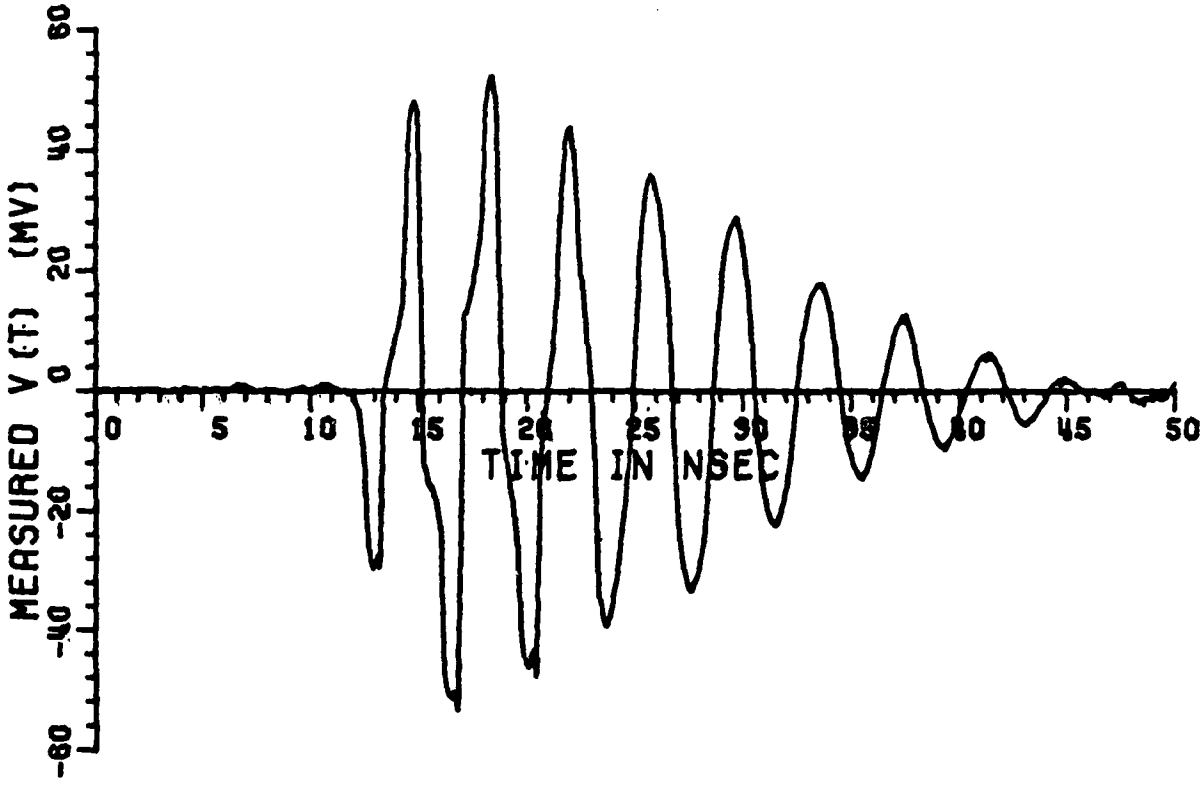

Figure 29. Measured laser-excited transient response of a thin wire excited at the tip.

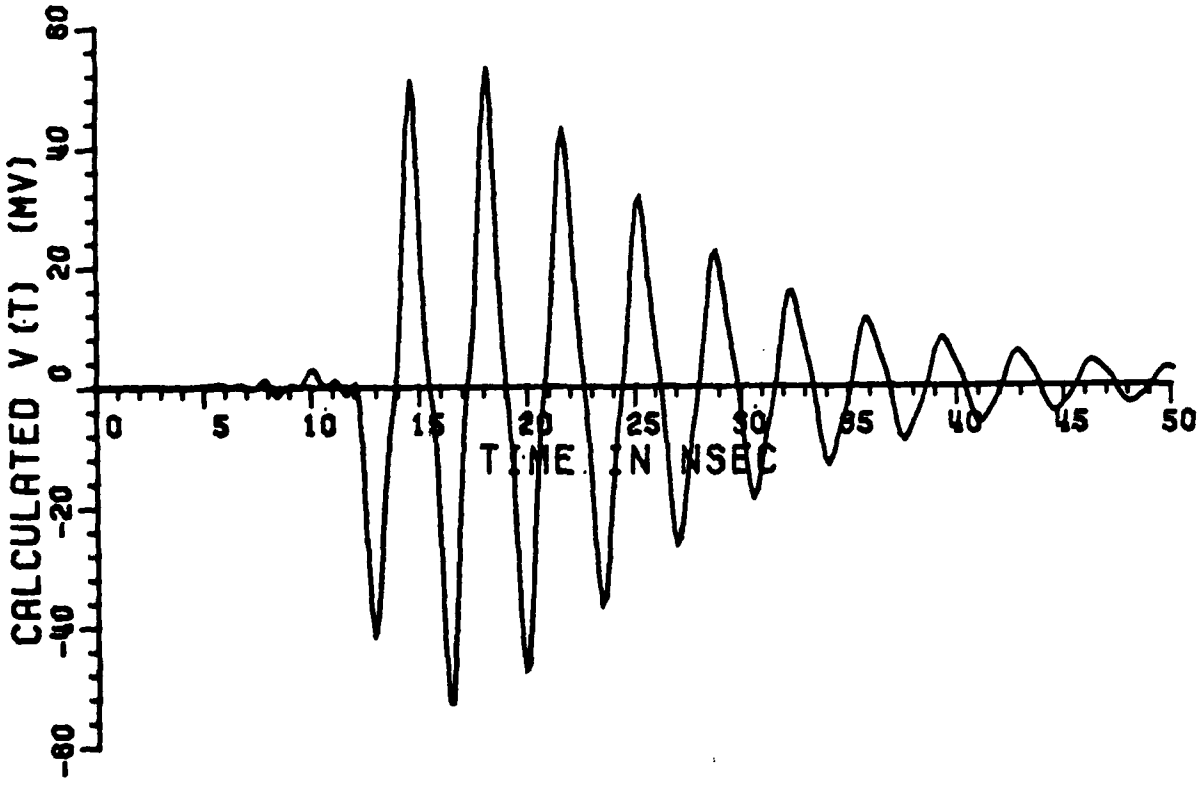

Figure 30. Calculated transient response of a thin-wire, tip excitation.

produced by a plane wave incident on the target, assuming the physical optics approximation for target scattering. Since a ramp response is simply derived from impulse response data, the crucial question concerning imaging is the validity of the physical optics approximation. A simple experiment to test this assumption was performed on this contract.

The physical optics assumption was tested by examining the strength of the excitation of the laser-illuminated spot as the polarization and incidence angle of the laser beam were varied. A diagram of the target region of the experiment is shown in Figure 31. The laser beam was aimed at a small spot, located 2 cm away from a tall (3') monopole which is at the center of a 5' diameter ground-plane. For the time intervals of interest, the monopole and ground plane are approximately infinite. (The edge and tip reflections happen several nsec after the initial coupled signal from the spot to the base of the antenna is finished.)

Initially, the incident laser beam was perpendicular to the ground plane. Then the direction of incidence was changed to 30^{o} and 60^{o} with respect to the normal, keeping the spot location fixed. A polarizing filter was present in the beam for all these experiments, and for the off-normal incidence angles, the polarization was rotated so that the incident optical E field was parallel to the plane containing the laser beam and the surface normal, and perpendicular to it.

The time-domain signals radiated by the spot were recorded on a transient digitizer, which was connected to the monopole. These magnitudes of the waveforms are plotted in Figure 32. It is estimated from these data that the magnitude is independent of polarization, and varies as the cosine of the angle between the surface normal and the laser beam. The cosine function is shown on the plot along with the data points. Given surface normal unit vector $\hat{n}$, output signal i(t), and

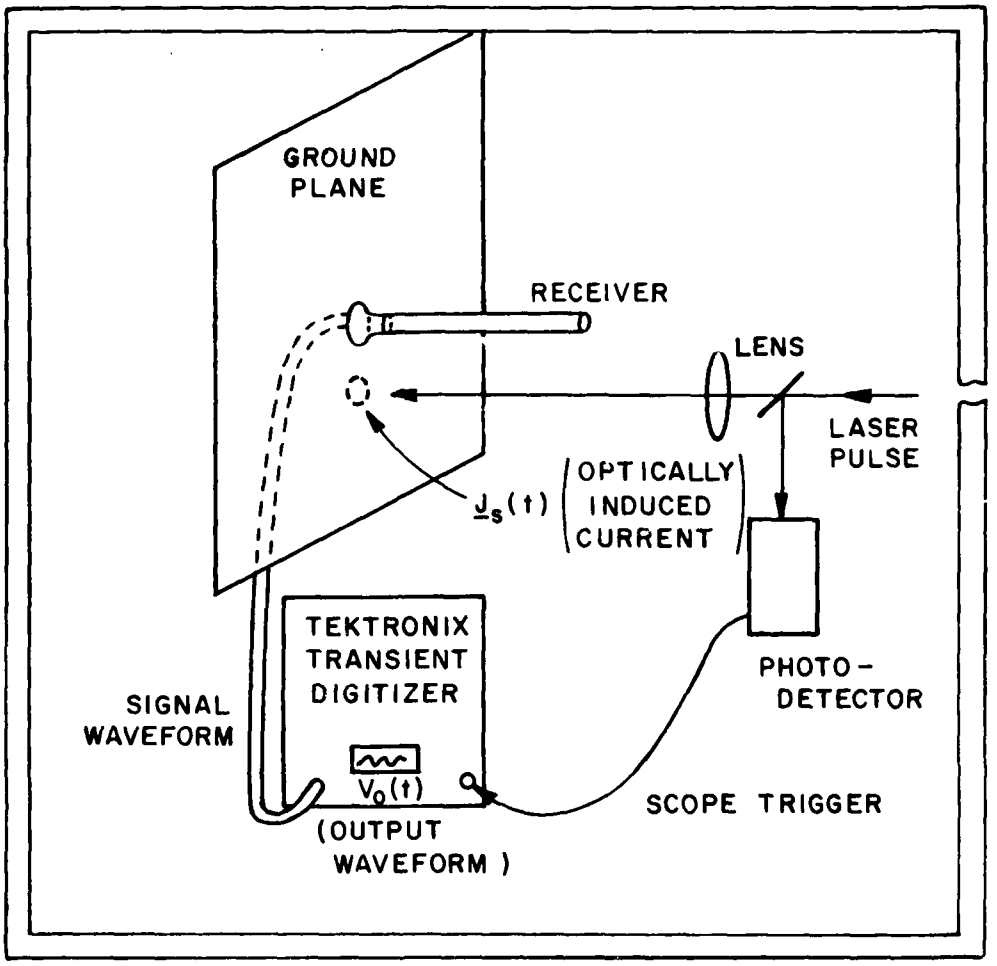

Figure 31. Diagram of experiment for measurement of laser-induced transients vs incident direction and polarization.

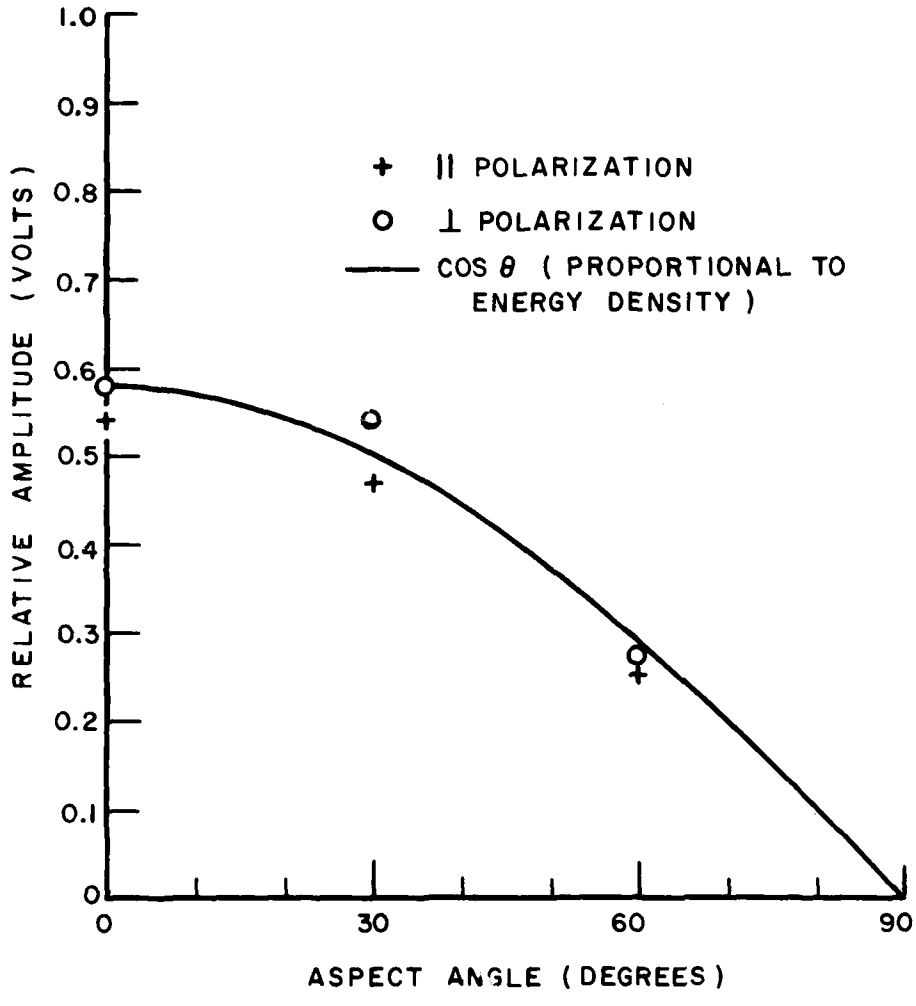

Figure 32. Relative laser-induced transient magnitude vs angle and polarization.

Poynting vector of the incident laser signal S(t), then $|i(t)|\alpha\hat{n}\cdot S_{inc}(t)$. As stated before, the source acts as a monopole, so that $i(t)=\hat{n}\ i(t)$, $\alpha\hat{n}(\hat{n}\cdot S(t))$.

Now the physical optics assumption states that for each spot on the surface, $i(t) = 2\hat{n} \times H_{inc}(t)$. Thus, this expression results in an $\overline{i(t)}$ which is a surface current, instead of being directed perpendicular to the surface. Furthermore, this expression predicts that $|i(t)|$ should be independent of incidence angle for the case where the H field is always parallel to the surface. Therefore, it is concluded that the physical optics approximation <u>does not apply</u> for the transient response signature excited by a strong laser pulse. If a powerful laser could be built such that a whole target (rather than just one spot) would be excited by the laser beam washing over its surface, then the backscattered electromagnetic transient response would contain reverberations which were characteristic of the target size and shape, but its initial time domain portion would not be proportional to target cross-sectional area vs distances.

VI. SUMMARY AND CONCLUSIONS

This twenty-one month study dealt with measurement of transient scattering signatures of a variety of cone-like objects at near nose-on look angles, and creation of images and/or identification from these data.

Complex scattering cross-section vs frequency was measured using harmonic frequency and swept frequency equipment. Six target shapes were measured, with angles of incidence from 0^{o} (nose-on) to 30^{o}, and a 58:1 frequency bandwidth. Comparisons to predictions making use of several approximate analysis techniques were made. Also, transient response waveforms were derived from the data.

Limiting surface images of the targets were created from measured data. Advances were made in the imaging algorithm such that the process was made faster and less dependent on operator interaction.

The derivation and characteristics of physical optics inverse scattering processes were studied for application to these targets. The effect of data limited to within a "window" in frequency and aspect angles was treated. Cone parameter calculation from measured data, making use of insight gained from physical optics analysis, was studied.

The conclusions of this study are:

1. Valid signature data were obtained for the targets. Accuracy of 10% in amplitude and $\pm 10^{o}$ in phase are estimated for the frequency domain data over a 58:1 band.

2. The data permit identification of the different shapes, even through the chosen targets were especially difficult because they were all the same length. If seems that their basic conical shape was most evident in the time domain signature data, while differences such as sharp or rounded edges were most obvious in the frequency-domain plots.

3. The physical optics approximation appears to be valid in the time domain up to the shadow boundary (base) for these targets. The approximation as formulated by Bojarski ("two-sided") appears valid at low frequencies.

4. The GTD and equivalent current analysis techniques gave results which matched the measured data very well. Since these approaches concentrate on scattering by the base, this must be the dominant scattering feature at near nose-on look angles.

5. It has been demonstrated that images of the targets can be automatically produced from the narrow range of measured data obtained on this program. The images clearly show the gross target characteristics. However, even with broadband signature information, the images do not have sufficient resolution to distinguish small target differences - such as rounded vs sharp edges and tips.

6. Based on the physical optics approximation the following target characteristics can be distinguished from the measured data
   a. target base diameter
   b. target cone angle.

7. Meaningful transient signatures can be excited by intense laser pulses incident on the targets. However, these signatures are not equal to or directly related to the impulse, step or ramp response signatures as commonly defined. Thus this area appears most useful for laboratory target signature research, and target identification, rather than for target imaging as used here.

Further research in several areas is recommended:

1. Transient signatures should be measured for several other target shapes, and also for the complete range of aspect angles on the present cone target models. These fundamental data permit further advances in analysis techniques, and also permit calculation of specific scattering response waveforms for any particular interrogating signal.

2. Additional effort toward improving and generalizing the measurement technique seems justified, particularly for more complex target measurements. The approach which uses subtraction of background scattering has been quite successful, and now target positioning and antenna selection and positioning can be concentrated

on. Furthermore, this approach is capable of measuring bistatic scattering signatures at arbitrary look angle combinations. These data would be very important in system evaluations for bistatic radars which are of current interest.

3. The limiting surface imaging technique using measured ramp response data deserves further investigation. One area involves its possible application to more complex shapes in free space. Another area involves imaging of underground targets from underground transient radar returns. Finally, this technique, or one related to it, may be of use for processing of over-the-horizon return data.

4. The laser excitation of transient electromagnetic signatures should be investigated further. A complete understanding of the physical process is important. This area has potential as both a tool for detailed laboratory scattering signature study, and long range remote sensing.

5. Broader understanding of the characteristics of physical optics inverse diffraction should be pursued. Incorporation of some terms approximating diffraction mechanisms into the physical optics model might make a meaningful improvement in its accuracy.

REFERENCES

References 1 through 4 were prepared by The Ohio State University ElectroScience Laboratory, Department of Electrical Engineering under Contract DAAG-77-C-0019 for U. S. Army Research Office.

1. J. D. Young, R. A. Day, F. R. Gross, E. K. Walton, "Basic Research in Three-Dimensional Imaging from Transient Radar Scattering Signatures," Report 784785-1, July 1978.

2. R. A. Day, "Automated Imaging of Cone-Like Targets from Transient Signature Data," Report 784785-2, March 1979.

3. E. K. Walton, "Broadband Scattering Signature Measurements of Cone Targets," Report 784785-3, July 1979.

4. F. R. Gross, "Application of Physical Optics Inverse Diffraction to the Identification of Cones from Limited Scattering Data," Report 784785-4, July 1979.

5. E. K. Walton and J. D. Young, "Radar Scattering Measurements of Cones and Computation of Transient Response," submitted to IEEE, AP-S, April 1979.

6. Radar Target Identification, Short Course Class Notes, Ohio State University, Department of Electrical Engineering, September 1977.

7. C. W. Chuang and D. L. Moffatt, "Natural Resonances of Radar Targets via Prony's Method," IEEE Trans. on Aerospace and Electronic Systems, Vol. AES-12, No. 5, pp. 583-589, 1976.

8. J. D. Young, "Measurement and Analysis of Spectral Signatures," Report 3387-1, July 1973, The Ohio State University ElectroScience Laboratory, Department of Electrical Engineering; prepared under Contract F04701-72-C-0180 for Space and Missile Systems Organization.

9. J. D. Young, "Target Imaging from Multiple-frequency Radar Returns," Report 2768-6, June 1971, The Ohio State University ElectroScience Laboratory, Department of Electrical Engineering; prepared under Grant No. AFOSR-69-1710 for Air Force Office of Scientific Research.

10. N. N. Bojarski, "Inverse Scattering," Final Report to Contract N00019-72-C-0462, Department of Navy, Naval Air Systems Command, April 1975.

11. N. N. Bojarski, "Signal Processing Studies and Analysis, Vol. IV - Three Dimensional Electromagnetic Short Pulse Inverse Scattering," Contract No. AF30(602)-3961, Syracuse University Research Corporation, November 1968.

12. E. M. Kennaugh and D. L. Moffatt, "Transient and Impulse Response Approximations," Proc. IEEE, Vol. 53, pp. 898-901, August 1965.

13. N. N. Bojarski, "Signal Processing Studies and Analysis, Vol. VII - Three-Dimensional Electromagnetic Short Pulse Inverse Scattering with Equatorial Derivative Scattering Data," Contract No. AF30(602)-3961, Syracuse University Research Corporation, November 1968.

14. N. N. Bojarski, "The Improvement of Electromagnetic Inverse Scattering Approximations," Contract No. AF30(602)-3961, Syracuse University Research Corporation, February 1967.

15. R. M. Lewis, "Physical Optics Inverse Diffraction," IEEE Trans. on Antennas and Propagation, Vol. AP-17, No. 3, pp. 308-314, May 1969.

16. R. D. Mager and Norman Bleistein, "An Examination of the Limited Aperture Problem of Physical Optics Inverse Scattering," Contract N0014-76-C-0039, Univeristy of Denver, Denver Research Institute, August 1976.

17. R. D. Mager and Norman Bleistein, "An Approach to the Limited Aperture Problem of Physical Optics Far Field InverseScatttering," Contract N0014-76-C-0039, University of Denver, Denver Research Institute, August 1976.

18. W. L. Perry, "On the Bojarski-Lewis Inverse Scattering Method," IEEE Trans. on Antennas and Propagation.

19. J. D. Young, "Measurement and Analysis of Spectral Signatures," Report 3387-1, July 1973, The Ohio State University ElectroScience Laboratory, Department of Electrical Engineering; prepared under Contract F04701-72-C-0180 for Space and Missile Systems Organization.

20. A. A. Ksienski, Y. T. Lin and L. J. White, "Low Frequency Approach to Target Identification," Proc. IEEE, Vol. 63, No. 12, pp. 1651-1660, December 1975.